Fluorine, lithium, caesium enrichment in Beiras Group spotted slates around the Cabeço de Argemela hyper-differentiated intrusion (Portugal)

Michel Cathelineau, Ícaro Fróis Dias da Silva, Marie-Christine Boiron, Gnienneman Yeo, António Mateus, Chantal Peiffert, Ivo Martins

Fluorine, lithium, caesium enrichment in Beiras Group spotted slates around the Cabeço de Argemela hyper-differentiated intrusion (Portugal)

Michel Cathelineau a,*, ´Icaro Frois Dias da Silva b, Marie-Christine Boiron a, Gnienneman Yeo a, Antonio Mateus b, Chantal Peiffert a, Ivo Martins b

a Université de Lorraine, CNRS, GeoRessources, 54506, Nancy, France
b Universidade de Lisboa, Faculdade de Ciencias, Instituto Dom Luiz, Campo Grande, Ed. C1, Piso 1, 1749-016, Lisboa, Portugal

Abstract:

The hyper-differentiated Cabeço de Argemela granite generated a well-preserved hydrothermal alteration halo within the spotted slates of the Beiras Group, offering an exceptional case study of granite-related geochemical dispersion in metasedimentary host rocks. Bulk-rock geochemistry and mineral chemistry of major phyllosili- cates were investigated along a profile extending south-eastward from the intrusion, combining petrography, micro-XRF mapping, EPMA and LA-ICP-MS analyses.

A systematic mineralogical and geochemical zoning is observed away from the intrusion, from quartz-–tourmaline metasomatized slates in the proximal halo to muscovite–biotite assemblages in the semi-distal zone and weakly altered spotted slates at greater distances. Tourmaline contents in the proximal halo (0–20 m) reach approximately 15–37 wt%, reflecting intense boron metasomatism. Geochemical enrichments define a multi-element dispersion halo extending over several hundred metres. Boron and arsenic show the strongest enrichments, with concentration increases of up to 70–100× and 150–200× relative to background values, respectively. Lithium is enriched by factors of 40–70, whereas caesium, tin and tungsten display more moderate enrichments (15–30×).

The alteration and geochemical dispersion are structurally controlled by the regional S0-S1 fabric, which acted as a pervasive permeability network during fluid circulation. Beyond the strongly metasomatized contact zone, lithium and fluorine emerge as effective pathfinder elements. Threshold values of approximately 1000 ppm B, 350 ppm Li and 2000 ppm F, corresponding to the outer semi-distal halo, are proposed as practical indicators for the detection of concealed, lithium-rich granitic intrusions in metasedimentary terrains.

Keywords : Beiras Group slates, Argemela lithium Fluorine, Water-rock interaction, Cordierite spots, LA-ICP-MS

1. Introduction

The impact of hydrothermal processes linked to intrusions of hyper- differentiated granites reveals that their host rocks can undergo several changes, both mineralogical and geochemical (Puchner, 1986; Arrykul et al., 1988; Chork, 1990; Gonçalves et al., 2018; Large and McGoldrick,

1998; Uribe-Mogollon and Maher, 2018). These mineral trans- formations and geochemical anomalies can then be considered as remote indicators of the proximity of metal-fertile intrusions. In the Portuguese domain of the Iberian Massif, within the Variscan Belt (Fig. 1a), a pioneering study in this field concerns the Regoufe W-specialised granite. There, a clear imprint of hydrothermal processes on mineral assemblages and total rock chemistry has been demonstrated by Haar et al. (1993). The Sn, F, B, Be (W, P, Ca minors) suite is thought to be typical of the intrusion itself. The fluids associated with the W mineralization hosted in the granite are considered the source of the Sn, F, B, W, Cs, and Rb enrichments recorded in the first 500 m around the intrusion.

The world-class Panasqueira deposit, located in the southern Central Iberian Zone (Fig. 1b), consists of a dense network of gently dipping quartz-wolframite veins hosted in Ediacaran slates surrounding a late-Variscan granitic system (Kelly and Rye, 1979; Bussink, 1984; Polya, 1989; Polya et al., 2000; Marignac et al., 2020; Mateus et al., 2020; Martins et al., 2022). Numerous studies have documented extensive hydrothermal alteration and associated geochemical dispersion in the host rocks (Oosterom et al., 1984; Gonçalves et al., 2018; Launay et al., 2021). Within approximately 1 km of the granitic cupola, tungsten and tin anomalies reach up to 60 ppm and 110 ppm, respectively, and are structurally controlled by brittle fault systems. In addition, multi- element enrichments in F, Li, Rb, Cs, As and W have been described, extending over several kilometres (Polya, 1989; Pinto, 2014; Codeço et al., 2021). These studies highlight the complexity of overlapping magmatic and hydrothermal processes, leading to large and heterogeneous geochemical halos controlled by both fluid evolution and structural pathways.

Such large and composite systems illustrate both the potential and the limitations of geochemical exploration in rare metal provinces.

While multi-element halos (e.g., Li, F, Cs, Nb, Ta, W) are widely recognized as key indicators of fertile granitic systems, their spatial dispersion and structural control may complicate vectoring towards mineralized centres. Recent developments in geochemical

prospecting increasingly emphasize the integration of multi-element signatures, mineral chemistry and alteration mapping to improve targeting of concealed rare metal intrusions.

In this context, smaller and structurally simpler systems, such as the Cabeço de Argemela intrusion, provide an opportunity to better constrain primary geochemical dispersion patterns associated with rare metal granites. The Cabeço de Argemela leucogranite plug has a com- plex sequence of magmatic processes (Michaud and Pichavant, 2020). Still, it has the advantage of being circumscribed and geometrically simple, with hydrothermal processes associated with a single magmatic mega-sequence. It represents an intrusion of a hyper-differentiated

magma of the Li (+Sn)-rich Rare Metal Granite (RMG) series, with

geochemical characteristics similar to the Lithium-Caesium-Tantalum (LCT) pegmatite swarms of the Central Iberian Zone (CIZ) (Michaud et al., 2020; Errandonea-Martin et al., 2022). Such systems are widely documented worldwide, including major deposits such as Tanco (Can- ada), Greenbushes (Australia), and Baishawo (China), and are typically associated with highly evolved peraluminous granites enriched in Li, Cs, Ta, Nb, Sn, and F.

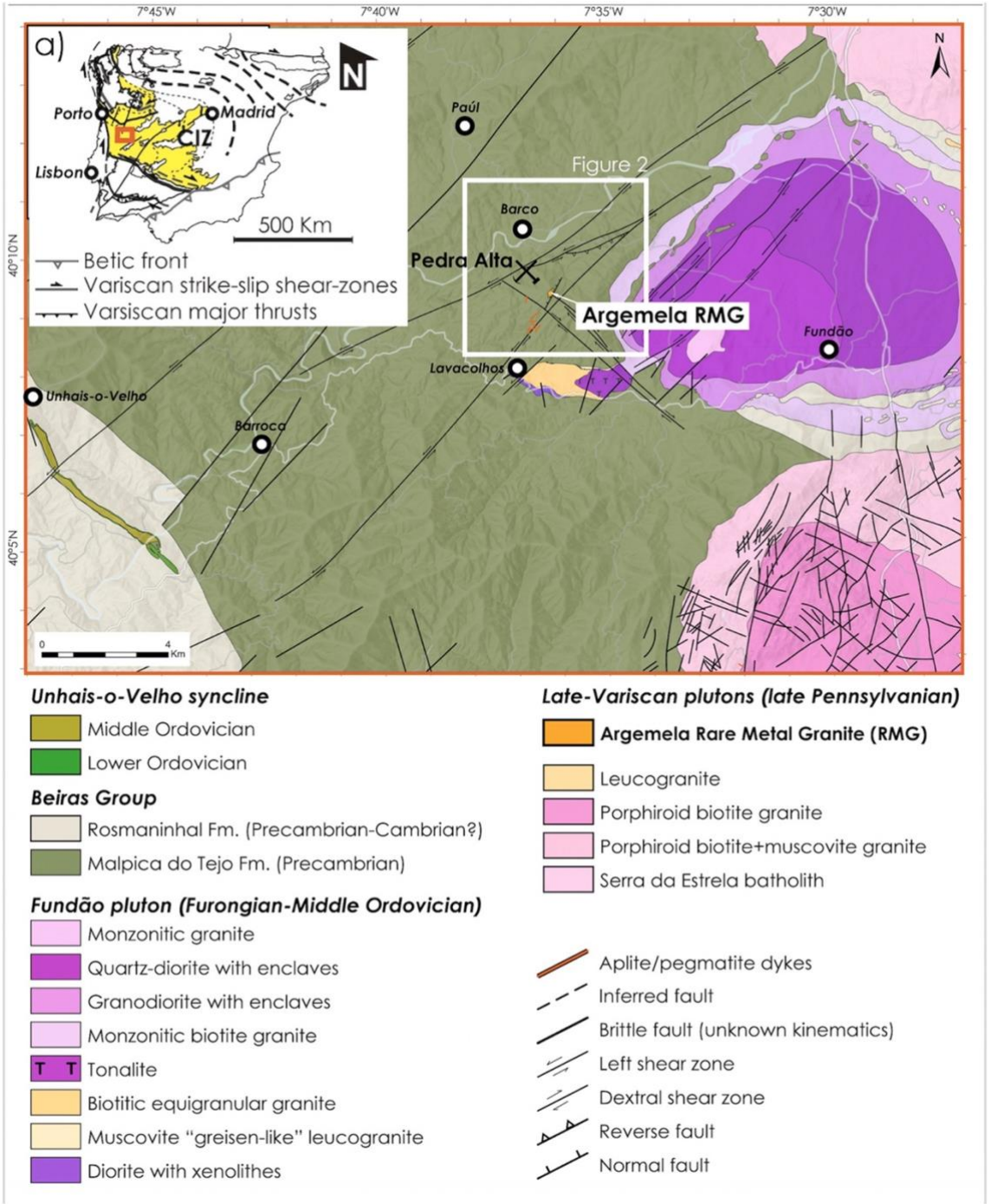

Fig. 1. Location of the studied area (Fig. 2) in the Iberian Massif and the Central Iberian Zone (CIZ) (a) and in the Panasqueira-Argemela sector (b).

This work aims therefore to describe, for the first time, the mineralogical and geochemical zonation surrounding this intrusion to understand the mineralogical, textural, and compositional changes of the hosting spotted slates that define the contact metamorphic aureole of a cryptic late-Variscan granitic intrusion and the Cambrian-Ordovician Fundã˜o pluton, exposed to the East. The spots are often considered to be andalusite or cordierite, now highly retro-metamorphosed, without verifying the sequence of processes that led to the currently identifiable mineral assemblages. In addition, the area showing spotted slates could be subject to a controversial interpretation in the case of several intrusions, and the relationships with deformation could be essential to understanding. Thus, Festa et al. (2013), using the example of the Serre massif (South Italy), consider that deformation related to pluton emplacement may propagate more than 3000 m from the intrusive contact, i.e., a wider domain than that of the contact metamorphism assemblages. The advantage of studying the host rocks of the Cabeço de Argemela intrusion lies in the fact that they are better preserved and exposed than those of Regoufe or Panasqueira, as they are not intersected by numerous mineralized quartz veins. The exception is the area located to the northwest near the Pedra Alta Sn/W mine (Yakovenko et al., 2025), which was excluded from the present study. The near-absence of mineralized veins and structures across the SW-N sector of the Argemela intrusion indicates a very limited potential for developing a mineralized vein system, which is precisely why this sector was selected. This choice allows the characterization of a continuous alteration halo without overprinted effects related to structurally controlled mineralization. Thus the main goal of this study was to document the geochemical impact of magmatic-derived fluids released during granite emplacement on surrounding metamorphic rocks. Specifically, the objective was to estimate the critical distance of water-rock interactions associated with the Argemela intrusion, within its tectonic and meta- morphic aureole context. Such a distance could be a tool for exploiting geochemical anomalies in metamorphic series and searching for con- cealed intrusions.

2. Local geology

The Cabeço de Argemela Rare-Metal Granite (Fig. 2) is a vertical, cylindrical pipe-shaped hypabyssal intrusion approximately one kilometre deep, as revealed by gravimetric data (Ribeiro, 2017; Michaud et al., 2020; Michaud and Pichavant, 2020). This intrusion comprises a main albite-rich middle-grained equigranular to porphyritic granitic facies composing the core and an edge unit consisting of a complex alternation of aplitic to pegmatitic facies. All

facies are cut by quartz- dominated veins (Charoy and Noronha, 1996; Inverno et al., 2019; Breiter et al., 2022). The porphyritic to microlithic textures of the granites are partially deformed, with evidence of cataclasis and sub- granular quartz under thin section. The Cabeço de Argemela core facies are characterised by the mineral assemblage quartz-albite-muscovite- lepidolite-Li phosphates-cassiterite and a magmatic-hydrothermal sys- tem that includes quartz and amblygonite comb-like veins (exclusive within the Cabeço de Argemela core and rim facies) and milky quartz- lodes with wolframite (Lima et al., 2019, also found cutting the spotted slates in Pedra Alta mine). The signature of this Sn-Li-(Nb–Ta) and W-poor intrusion brings this type of magma closer to those involved in the Lithium-Caesium-Tantalum pegmatites of the Central Iberian Zone.

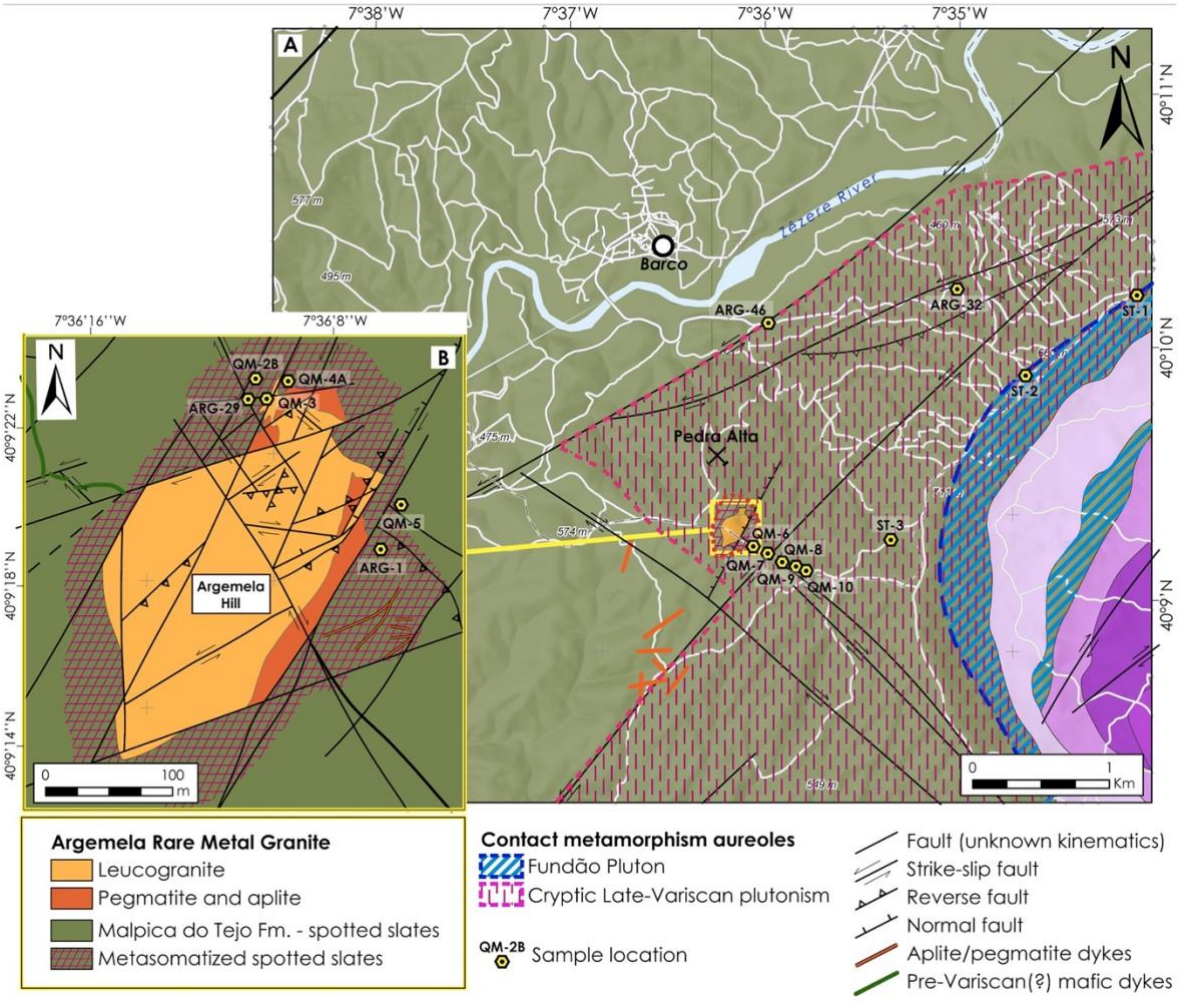

Fig. 2. a) Geological map of the western section of the Fund˜ao Pluton, with the main shear zones and faults, the contact metamorphic aureoles, and sampling locations. Mapping based on original and published data (Portugal Ferreira et al., 1977; Inverno et al., 2019; Meireles, 2020); b) Detailed map of the Argemela Rare Metal Granite, with main structures, metasomatic halo, and sampling locations. The Panasqueira and Argemela area is bracketed between the N130-140° E trending, Variscan Unhais-o-Velho syncline underlined by the kilometre-long lower Ordovician Armorican Quartzite to the west, and a series of granitic plutons (Figs. 1 and 2): to the north, the Pennsylvanian-early Permian granitic intrusions of the Serra da Estrela (Sant'Ovaia et al., 2010) and, to the East, by the Furongian-Early Ordovician Fundá˜o pluton (Antunes et al., 2012). In this area, the Bei- ras Group of the Slate and Greywacke Complex (Ediacaran to lower Cambrian?) (Sousa, 1983) is represented by the Upper Member of the Malpica do Tejo Formation (Ferreira da Silva, 2013; Romã˜o et al., 2010), which comprises a flysch-type detrital sequence, with metric to milli- metric rhythmic alternations of pelitic and sandy lithologies, including fine to coarse-grained greywackes, lithic sandstones, and conglomer- ates. Mafic and felsic sub-volcanic, highly deformed rocks are locally identified, cutting the metasedimentary sequence. Additionally, unde- formed aplite dykes are observed in the region, locally clustering in dyke swarms (Fig. 2), which include other aplite geometrically irregular in- trusions, often highly weathered and cut by brittle faults.

Michaud (2019) and Michaud and Pichavant (2020) examined the deformational effects of granite intrusion on the surrounding slates. They noted a deviation in cleavage attitudes near slate-granite contacts, particularly with the Cambro-Ordovician Fund˜ao pluton, which pro- duces a large-scale strain shadow. By studying folds and axial-planar cleavage, they proposed a dispersion of cleavage directions compared to the regional trend. The study also reveals dextral shearing processes along the NE apophysis of the Argemela granite, which affect the adja- cent shales and form sigmoidal-shaped textural arrangements. The contact zones between the granite and the slates show alternating parallelepiped slabs and are influenced by sub-vertical intrusive con- tacts and vertical shear zones. They suggest that the location of defor- mation may have caused the chimney-shaped intrusion in the shape of a clockwise chimney. According to Michaud et al. (2020), in the restricted Argemela area, the main foliation directions are distributed in different sectors, NW-SE as usual in other parts

of the region, in the northern area of the Cabeço de Argemela intrusion, but N-S along the Serra do Gomes near the Fundã˜o granite, N100-130 in the northern part, and NW-SE to N-S in the southern part of the Argemela district.

There are, therefore, significant deviations from the usual NW-SE directions in the S and SW surroundings of the Cabeço de Argemela intrusion. All the published papers point to the hypothesis of a concealed granite body below the Cabeço de Argemela plug. The presence of Sn-Li ores (Pedra Alta) to the NW of the Argemela plug has been the subject of controversies about the links with magmatic intrusions. In most studies, it is hypothesised that the Sn-Li quartz lodes of Pedra Alta should not be genetically linked to the Cabeço de Argemela granite, but in both cases probably associated with a common parental intrusion at depth (Inverno and Ribeiro, 1980; Charoy and Noronha, 1996; Inverno et al., 2019). The main differences in hypotheses lie in how this deep body is related to, or genetically linked with, the exposed composite batholiths nearby (Fundão, to the East, considered as much older, and Serra da Estrela, to the North). However, the hidden granite body might represent a separate batch of anatectic granite magma at depth, independent from the Serra da Estrela composite batholith and any outcropping granites (Michaud, 2019). From the Cabeço de Argemela to the Fundão pluton, slates are mainly spotted, with few gaps of non-spotted areas. According to Inverno et al. (2019), the origin of the spots in the slates would be either the intrusion of the Fundão granitoids to the SE or, in the case of slightly biotite-mottled slates in the north-west of the Cabeço de Argemela intrusion, a cryptic late-Variscan granitic dome at shallow depths, which could be revealed by the radiometric anomalies and a circular structure with a weak signal on Landsat 2 images (Santarém, 1983).

3. Materials and methods

3.1. Sampling

For this study, a total of 16 samples were collected in the Argemela- Fundão pluton area (Fig. 2 and Supp. Table 1). The selected sites were constrained by the detailed geological mapping presented in this work. Some of them were chosen to have a well-constrained sampling profile that allows for characterising the mineral and chemical modifications experienced by the Beiras Group slates from the regional background (spotted and unspotted slates; Fig. 2a) towards the exposed section of the Cabeço de Argemela RMG and its metasomatized halo (Fig. 2b). It is worth noting that vertical sampling profiles cannot be designed because there are no boreholes far enough from the Argemela intrusion, and no other options exist for vertically sampling the surrounding metasedimentary rocks. The lateral profile carried out is

therefore based on the assumption that the alteration halo formed more or less evenly around the intrusion, an assumption often used in similar studies.

3.2. Analytical methods

Micro-X-Ray Fluorescence (micro-XRF) images of slates and SEM images were obtained on thin sections to establish the paragenetic sequence and before chemical analysis of minerals. Micro-XRF mapping, SEM, and Electron microprobe analyses (EPMA) were performed at the SCMEM analytical platform (GeoRessources, Nancy, France). Details about the analytical conditions for micro-XRF, SEM and EMPA can be found in Cathelineau et al. (2024). A Bruker-Nano M4 Tornado instrument equipped with an Rh X-ray tube (Be side window) and poly-capillary optics, giving an X-ray beam with a 25-30 μm diameter on the sample was used to obtain micro-XRF chemical maps. The X-ray tube was operated at 50 kV and 200 μA. Two 30 mm^2 Xflash® SDD detectors
measure X-rays with an energy resolution of ⩽135 eV at 250,000 cps. All analyses were carried out at a 2 kPa vacuum.
A JEOL JSM-7600F Schottky-FEG-SEM equipped with an Oxford Instruments 20 mm2 SDD-type EDS spectrometer was used for the SEM images. For EMPA, the analytical conditions of the CAMECA SX100 EPMA were accelerating voltage of 15 kV, probe current of 12 nA and beam diameter of 1 μm.
Muscovite, biotite, and chlorite were analysed with LA-ICP-MS at GeoRessources to determine the trace element concentrations. Laser ablation utilised an ESI New Wave Research UC 193 nm excimer laser at a frequency of 10 Hz. The ablated material was carried by helium gas (0.65 l.min-1), which was mixed with argon (0.9 l.min-1) before entering the ICP torch and analysed with an Agilent 7900 ICP-MS. External calibration was carried out using the NIST 610 and 612 glass standards. Si was used as an internal standard to calculate absolute concentrations in muscovite, biotite, and chlorites. The Iolite software (version 4) (Patton et al., 2011), following the standard methods re- ported by Longerich et al. (1996) was used for data reduction.
Whole-rock major and trace element analyses of collected rock samples were done at SARM, the National Laboratory for rock analysis from CNRS (Centre national de la Recherche scientifique) at CRPG(Nancy, France). Major elements were analysed by inductively coupled plasma optical emission spectrometry on a Thermo-Fischer ICap 6500

instrument. Trace elements, including rare earth elements (REE), were determined by inductively coupled plasma mass spectrometry (Thermo- Elemental X7). Li, F and B were analysed by wet chemistry, using atomic absorption. Detailed analytical procedures are provided in Carignan et al. (2001).

4. Results

4.1. Mapping of deformation

New geological maps were established on the area covering the Cabeço de Argemela intrusion and its surrounding Malpica do Tejo Formation (Beiras Group) to the Fundão pluton in the East (Figs. 2 and 3). A succession of local deformational events has been determined. In the mapped area, the Beiras Group metapelites and coarser-grained detrital rocks underwent a strong and pervasive deformation (D1) that produced tight isoclinal folding with axial plane sub-vertical cleavage (S1), transposition of bedding by crenulation and pressure solution, and formation of strike-slip ductile-brittle shear zones (Fig. 3). This compositional layering, characterised by diffuse and gradual boundaries and root-shaped morphologies, is the regional and dominant foliation encircling the Cabeço de Argemela intrusion and represents a tectono- metamorphic layering that has been poorly characterised to date. This transposed fabric is contemporaneous with biotite blastesis, which marks the thermal peak of the Barrovian metamorphism in this area, predating the spots (porphyroblasts) in the contact metamorphism aureoles associated with Variscan and Lower Palaeozoic plutonism in this sector. Despite the vertical and lateral facies variations recorded by the Malpica do Tejo Formation, which could be locally strong, compiled evidence shows that pelite/siltite laminations and greywacke- microconglomerate beds interfaces indicate a NW-SE transposed bedding (S0//S1) with steep dipping (varying from 70° SW to 70° NE, with 85° SW on average). These laminations decrease in thickness along strike, eventually tapering off, evidencing the tectonic obliteration of the bedding, sometimes at low angles in the coarser-grained beds or trans- posing it entirely in the most pelitic strata.

The S0//S1 compositional layering is affected by a gentle folding event (D2) that produced vertical axis folds with an NNW-SSE to NNE-SSW steeply dipping axial plane crenulation cleavage (S2; 77° WSW on average) (Fig. 3). D2 folds and S2 cleavage are better developed in the most pelitic layers. The intersection of S1 and S2 is a vertical lineation, which is subparallel to the D2 fold axis. The observed D2 structures are geometrically compatible with those also ascribed to the regional late-Variscan third deformation phase (Marques et al., 2002).

The youngest deformation stage (local D3) has produced centimetre to metre-spaced subhorizontal crenulation. It folds with a rough axial plane pressure-solution cleavage (S3), cutting the previous fabrics with a very heterogeneous distribution (Fig. 3). These sub-horizontal kink-bands and joints seem to be closely related to near-vertical, E-W to NNE-SSW brittle faults (Fig. 3) with associated sub-vertical kink-bands, also cutting the (local) D1 and D2 fabrics and the latest magmatic intrusions (undeformed aplites). The effect of these brittle structures on the dispersion of the attitudes of the main foliations (S1 and S2) is signifi-cant in this sector. This deformation stage postdates the spots in the Beiras Group slates and the metasomatic halo surrounding the Cabeço da Argemela RMG.

4.2. Petrography of enclosing rocks at Argemela

4.2.1. Proximal halo

The metasediments observed at the contact and over the first ten meters around the Cabeço de Argemela RMG intrusion are profoundly modified compared with slates outcropping more than one hundred meters away from the intrusion (Fig. 2a and b). The spotty character observed in most surrounding slates has been completely erased near the contact with the Argemela granite. The slates display a light greenish to greyish colour, derived from metasomatic effects (Fig. 4). On the northeastern contact, the metasedimentary rocks are highly silicified and, locally, multiple generations of quartz veins intersect the foliation (Fig. 4a and b). On the southern contact (Fig. 4c and d), the silicification is comparatively less intense. However, metasediments show dense networks of micro-fissures interconnected with the foliation planes (Fig. 4c). The foliation is still identifiable, being highlighted by darker edgings (Fig. 4b, c and d), which, as shown by the results of detailed petrographic studies, are tourmaline enrichments replacing the phyllo-silicates in the original spotted slates. In Fig. 5, some examples of intensified tourmalinization at the sample scale are

highlighted. Fig. 5a shows a domain of complete tourmalinization of the host rock minerals, which appears in black at contact with an intrusive aplite dyke traced by hydrothermal quartz aggregates. Fig. 5b exemplifies another quartz- tourmaline contact, and Fig. 5c shows the development of tourmalinization along the foliation planes, which appear as a very dark, dense network. In this sample (ARG-29b), the schist is silicified in the light grey parts at the northeast contact of the Argemela granite. Samples QM4 (3 m from the contact, Fig. 5d) and QM5 (44 m from the contact, Fig. 5e and f) show progressively less intense tourmalinization in comparison with the samples at the contact (Fig. 5d). In sample QM5, the spots in slates are evident as shown in its image pair (Fig. 5e and f), with a transmitted light photograph and a composite map of potassium and iron obtained by X-ray micro-fluorescence.

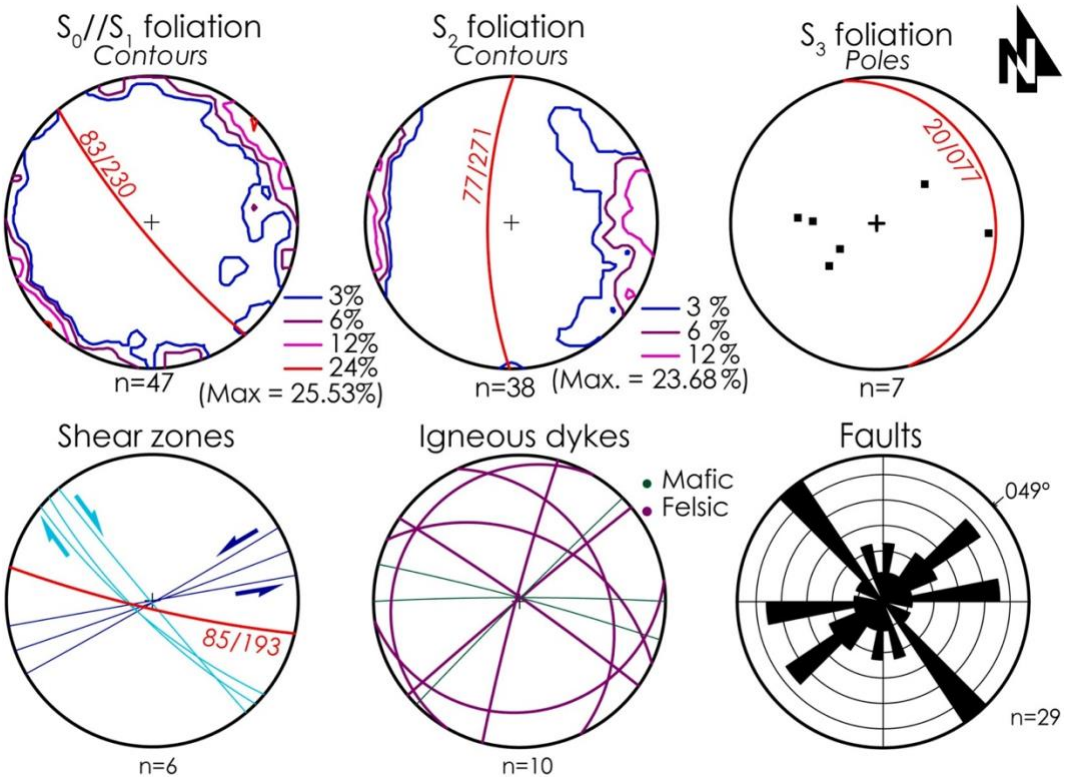

Fig. 3. Stereographic projections of the fabrics, faults and dykes identified in this area: S0-S1, S2 and S3 foliation of the slates at the left-hand side, and shear zones, igneous dykes, and faults at the right-hand side.

The profoundly modified slates of the first 15 m or so at contact with the intrusion were observed in detail using electron microscopy and X- ray microfluorescence. Sample ARG1 is particularly representative, showing a greenish-grey hue with an anastomosing network of

micro- cracks related to the foliation planes (Fig. 6a). The corresponding chemical maps (Fig. 6b, c, d) show that the blackish networks correspond to an iron-rich carrier (tourmaline). At the same time, the matrix is essentially composed of layers enriched in K-silicates and more siliceous and K-poor layers. Titanium oxides highlight the foliation planes along the K-rich layers. Observed with SEM, the darker beds correspond to an association of tourmaline and minor quartz-muscovite (Fig. 6e, f, and g). In contrast, the potassium-enriched layers correspond to an association of biotite and muscovite with a few isolated tourmaline grains (Fig. 6g and h). The tourmaline grains have small basal sections, varying in diameter between 10 and 20 μm.

4.2.2. The semi-distal metasomatic halo

Beyond 40 to 50 m from the Cabeço de Argemela RMG, slates are characterised by a compositional layering defined by quartz-rich and micaceous-rich bands, which show centimetre-sized retrogressed spots (Fig. 7a and b). These slate exposures thus display the characteristics of the mottled slates known on a regional scale, with spot density linked to the chemical-mineralogical nature of the metasediments (e.g., the pro- portion of metapelites versus sandy facies). Optical microscopy images reveal that the spots are zoned and surrounded by a finely crystallised matrix. They are greenish with a darker rim. The spots are not rounded or ellipsoidal. They are geometrically shaped here, and the pseudo- hexagonal basal sections are compatible with the ones expected for pinitized cordierite blasts (Fig. 7c and d, and micro-XRF corresponding chemical images, Fig. 7e and f). SEM images (Fig. 7g and h) indicate that the dark haloes in the spots consist mainly of well-crystallised biotite that is roughly perpendicular to the spot surface and variably chloritized.

In contrast with the dark rim, the spot core consists of an association of biotite (± chloritized) and muscovite. A mica-enriched edge is sometimes observed between the darker biotite rim and the core of mixed biotite-muscovite filling (Fig. 7 g and h). The fine-grained matrix surrounding the inferred cordierite crystals consists of quartz and muscovite (10-20 μm) with a few scattered biotite plates. Most of the

samples positioned between 40 and 200 m from the Argemela intrusion show the same mineral and textural characteristics.

As a preliminary conclusion, cordierite is entirely replaced by a K- mica-chlorite assemblage and is no longer preserved. This replacement is well documented at the microscale by optical microscopy and SEM

observations.

4.2.3. Distal samples

Samples picked farther from the Argemela intrusion in the sampling profile (Figs. 2 and 8) display facies attributes that are slightly different from those of the previous ones. The ST-3, -2, and - 1 (Fig. 8), which originate from slate exposures at the boundary or near the Fundã˜o pluton contact metamorphism aureole, are characterised by the presence of a relatively strong crenulation surrounding the porphyroblasts, which complicates the textures. Nevertheless, the mineralogical features observed across the intermediate segment of the profile remain the same. Locally, relics of andalusite have been found among the cordierite pinites.

To the north and east-hand side of the profile, the two samples show spots without zonation. They are larger (Fig. 8). In the ARG-46 sample, in contrast with ARG-32, pseudo-hexagonal spots exhibit strain shadows with almond shapes, probably due to strain accommodation by the influence of a neighbouring late-Variscan shear zone (Figs. 2 and 8). The presence or absence of post-cordierite blastesis crenulations appears to follow an erratic pattern. It is possibly related to the high heterogeneity of the local D2 and D3 deformations (folding and shearing) in the studied area.

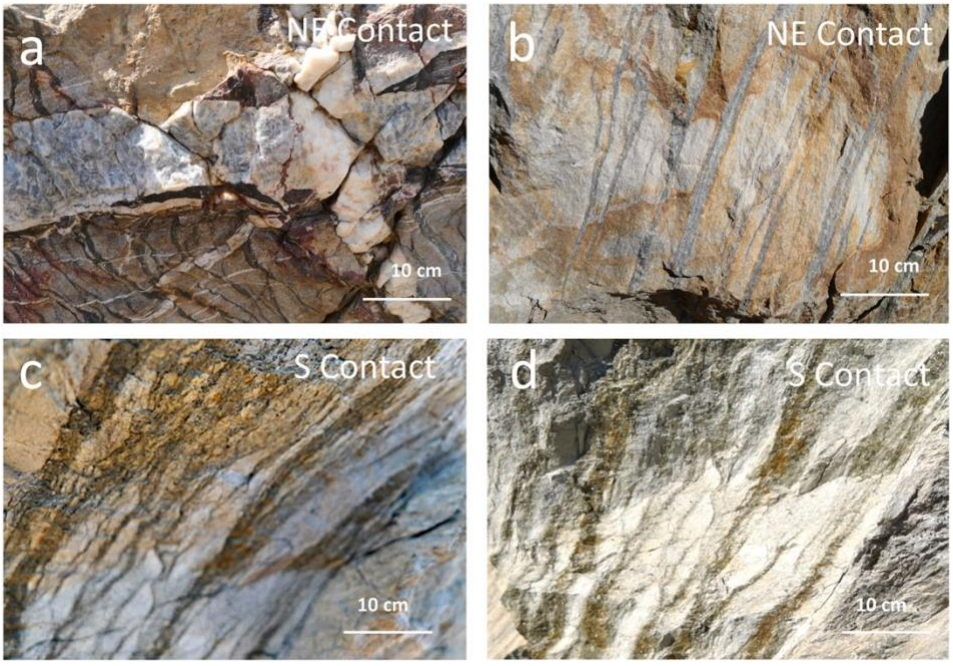

Fig. 4. Metasomatised slates near the contact with the Argemela intrusion: a and b: northeastern contact showing quartz veins in part inherited (folded milky quartz veins) and in part linked to the intrusion (fracture); c and d: southern contact, documenting the development of a tourmaline-rich network of micro-fissures relayed by the foliation planes in the quartz-rich beds.

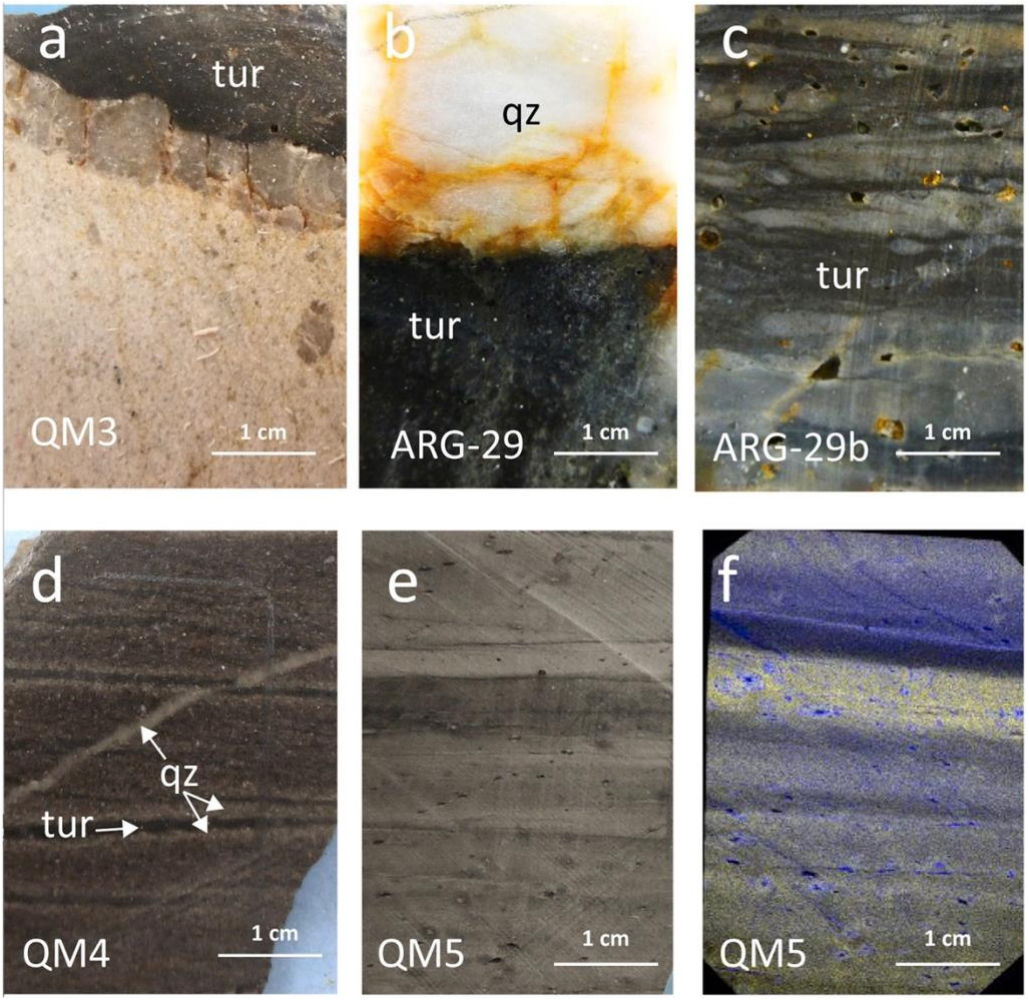

Fig. 5. Tourmalinised host slates near the contact with the Argemela intrusion. The presented sections are from the main profile from intrusion to the southeast (a, d, e, f: QM3, 4, 5), and ARG 29 and ARG-29b were taken close to the northeastern border of the intrusion. a: at the very contact with fine grained granite, a quartz vein is at the boundary with a slate entirely replaced by tourmaline; b: a contact with tourmaline in black and quartz at the very contact with the intrusion; c: tourmalinised slates with alternance of tourmaline rich and quartz rich layers; d: tourmalinised slates, with layers enriched in tourmaline (in black) surrounded by layers enriched in quartz, both in a quartz-muscovite matrix; f: fine-grained slate facies with tiny inclusions, mostly tourmaline, and free of large cordierite spots. Fig. 5f corresponds to the micro-fluorescence image of the sample from Fig. 5e. It shows the alternation of muscovite-rich (K-rich, as K appears in yellow) layers and iron- rich layers (Fe in blue), dominated by tourmaline (and minor biotite).

4.2.4. Mineral indicators and sequence

The mineral assemblages in the slates are as follows: i) quartz- tourmaline-muscovite-biotite in the proximal zone (proximal zone), ii) biotite-muscovite in the intermediate zone (semi-distal zone). The biotite plates are largely retro-metamorphosed into chlorite, but there is no doubt that the original platelets formed on the cordierite blasts were mostly of biotite composition.

The relative chronology of the mineral assemblages observed is fascinating. As noted earlier, the early formation of cordierite can be deduced from the shape of pseudomorphs when they are preserved. In reality, cordierite is completely replaced by a K-mica-chlorite mix and no longer exists. This transformation is clearly seen at the microscale through SEM observations. As a result, it is not possible to study diffusion processes in cordierite since the original mineral is gone, and the newly formed phyllosilicates are extremely fine-grained. Nonetheless, the successive complex transformations involving superimposed meta- morphic and hydrothermal histories can be interpreted as follows (Fig. 9): i) inheritance of supposed cordierite spots, now pinitized, ii) development of newly formed biotite around the spots, iii) retro-metamorphosis of the cordierite spots into a mica+biotite assemblage, iv) retro-metamorphosis of biotite into chlorite.

Using combined whole-rock geochemical data (Supp. Tables 2 to 4) and mineral composition analyses, it was possible to estimate the mass proportion of tourmaline in the alteration halos. In the proximal halo (0-20 m), tourmaline contents are estimated to range between approximately 15 and 37 wt%, with the highest value corresponding to the most strongly metasomatized facies (QM3). In the semi-distal halo (20-300 m), tourmaline proportions decrease markedly to about 2-7 wt %, whereas in the distal zone (>300 m), tourmaline contents are low and estimated between ~0.3 and 1.5 wt%. Tourmaline is therefore a pertinent mineral indicator of the proximity of the intrusion.

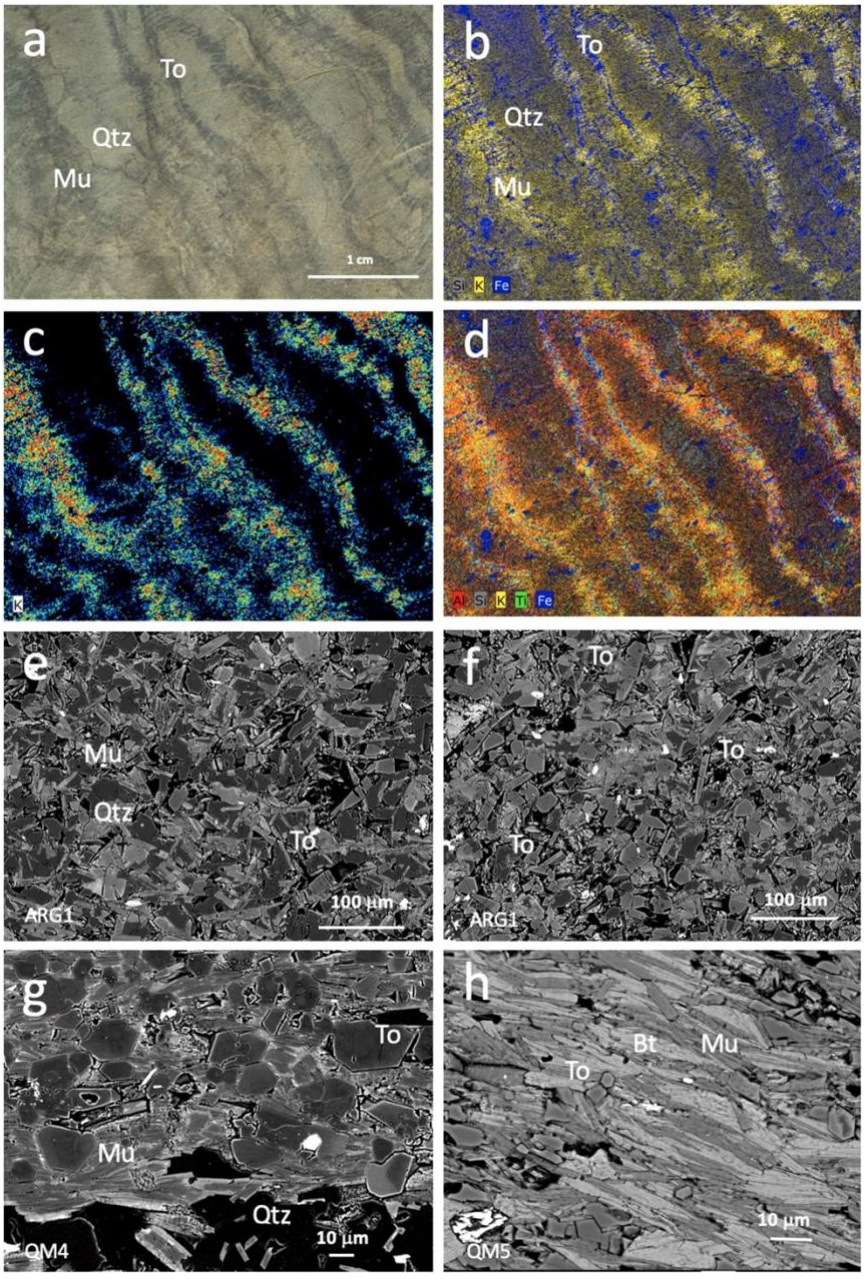

Fig. 6. Metasomatised (tourmaline-rich) slates near the contact with the Argemela intrusion: a and b: for the same sample, in a) the macroscopic texture, and in b) a composite chemical image with iron (blue) and potassium(yellow) showing the iron enrichment due to the tourmaline development in a muscovite-rich matrix. The two following micro-XRF images (c and d) are for potassium only, and a composite image for Al, Si, K, Ti, and Fe. e) to h) are SEM back-scattered images of the rock textures, particularly the quartz-muscovite (minor tourmaline) in the potassic layer; in f and g, the development of euhedral tiny tourmaline crystals with little zonation, and h) the biotite-muscovite association found in some layers.

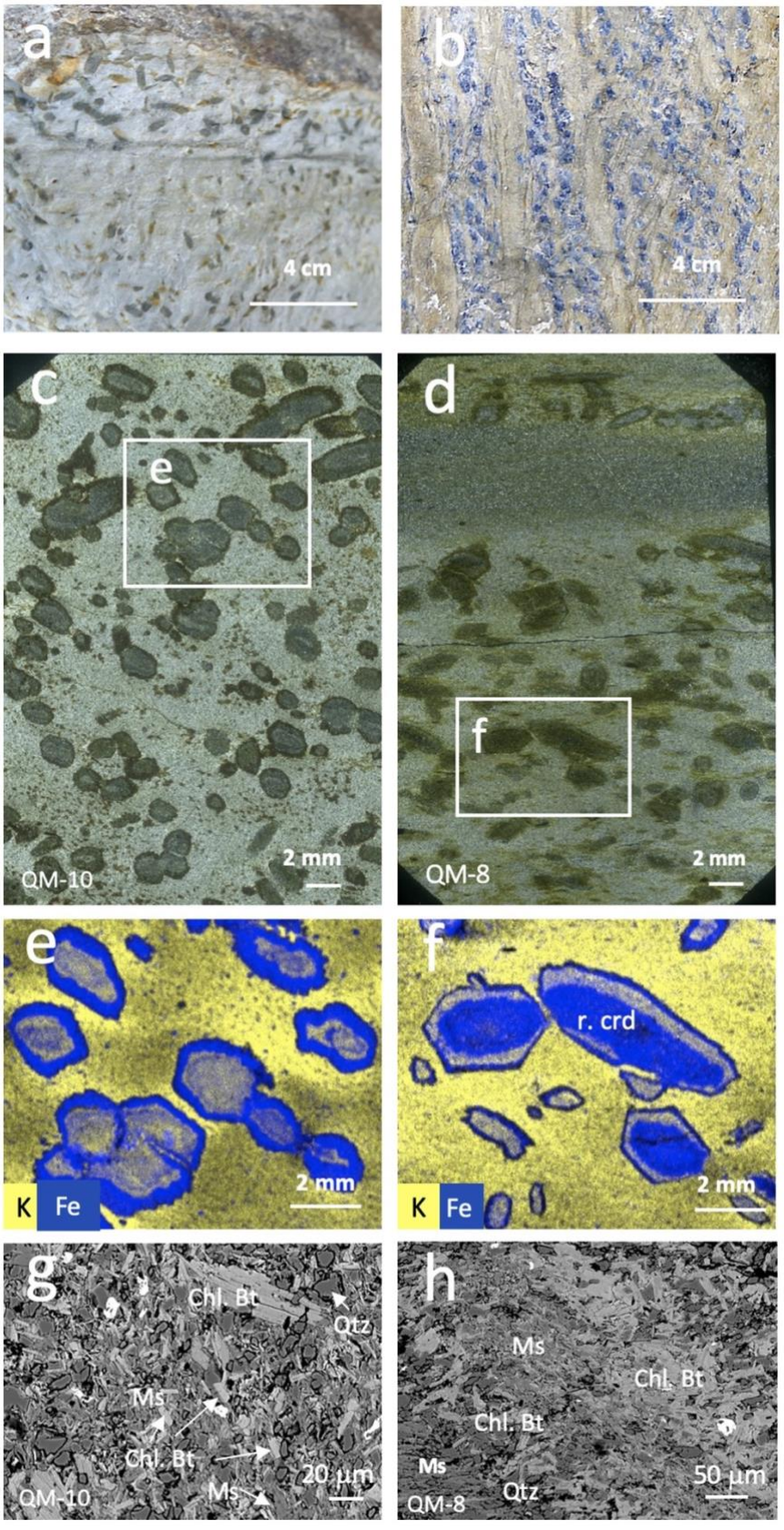
a
4 cm
b
4 cm
c
e
QM-10
2 mm
d
f
QM-8
2 mm
e
K Fe
2 mm
f
r. crd
K Fe
2 mm
g
Chl. Bt
Qtz
Ms
Chl. Bt
Ms
QM-10
20 µm
h
Ms
Chl. Bt
Chl. Bt
Ms
Qtz
QM-8
50 µm

Fig. 7. Mineralogy of spotted slate samples in the semi-distal halo: a) outcropping spotted slates with differences in the size of the spots; b) spotted slates showing the development of spots only in aluminous-rich layers; c) section of the QM-10 sample showing euhedral spots with pseudo-hexagonal shapes, and a darker rim; d) QM8 sample displaying spots in the aluminous-rich layers and the lack of spots in a quartz-rich layer; e) and f) are composite micro-fluorescence X chemical images of potassium and iron, corresponding to the white squares from c and d respectively; g and h are SEM backscattered electron images of the microscopic textures with: in Fig. 7g, the matrix dominated by micas with some biotite and quartz grains, and Fig. 7h the boundary of the spot made of biotite (chloritized) crystallised outwards or inwards on either side of the supposed cordierite crystal boundary.

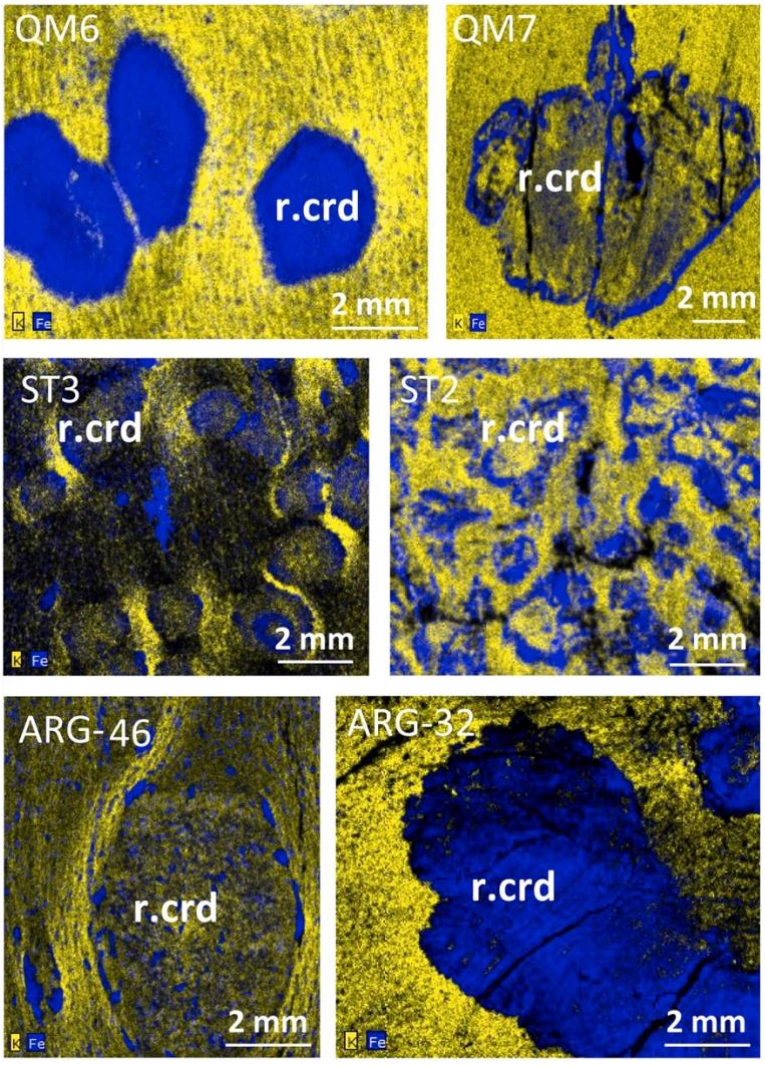

Fig. 8. Main textures of spotted slates (Beiras Group) along the profile from the Argemela intrusion to the East as revealed by micro-XRF with two elements (K and Fe). The colored inclusions in blue correspond to the retromorphosed cordierite (r.crd) crystal with a biotite-chlorite core or rim (rich in iron) in the mica matrix (rich in K).

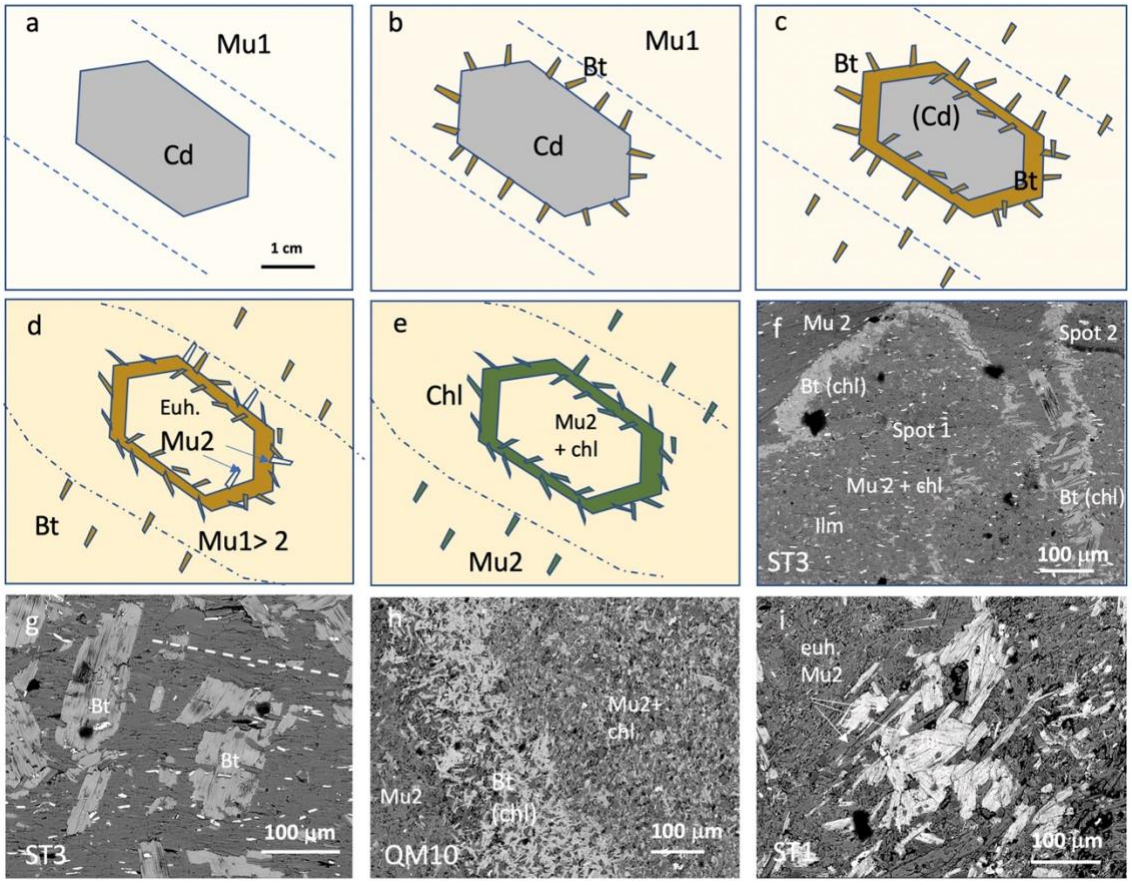

Fig. 9. Schematic representation of the chronology of mineral changes in the Beiras Group slates: a) cordierite-muscovite -biotite assemblage related to an inferred intrusion at depth, b) development of biotite onto the cordierite crystals first outwards and inwards (c) due to the progressive replacement of cordierite by a muscovite-biotite assemblage; biotite crystals grow perpendicular to the central foliation S0-S1 d) locally large muscovite crystals formed also on the boundary of the cordierite phantom, and crosscut also biotite crystals, e) finally, the biotite plates are entirely replaced by chlorite, leaving a chlorite-muscovite association, f) general view of two spots (noted spots 1 and 2) with the biotite rim and muscovite infilling with some crystals of ilmenite (ilm), g) example of biotite growth perpendicular to the main foliation indicated by a dashed line, h) rim of biotite around the core where muscovite (Mu1 recrystallized in Mu2) predominates, and j) development of euhedral muscovite plates Mu2 in open space.

In contrast, quantifying the relative proportions of muscovite and biotite (largely chloritized) is significantly more difficult. The abun- dance of phyllosilicates is strongly controlled by the primary lithological heterogeneity of the detrital sedimentary protolith,

particularly the proportion of quartz-rich versus pelitic layers, as well as by subsequent ductile deformation and recrystallization. Major element concentrations (e.g., SiO_2, Al_2O_3, FeO, MgO, K_2O) confirm this lithological variability and do not provide reliable quantitative markers for estimating phyllosilicate modal proportions. As a result, quantitative mineral pro- portion estimates are considered robust only for tourmaline, whereas mica proportions can be only discussed qualitatively in particular on the basis of micro-XRF image.

4.3. 4.3. Whole rock geochemistry

Whole rock analyses of the slate series in the profile are characterised by concentrations of major elements that are typical of shales in the Beiras Group, placing them into the "shale compositional domain" of most sedimentary facies classification schemes. There are no significant variations in major elements along the profile, and their concentrations reflect mainly the relative abundance of aluminous-rich and silica-rich layers. In contrast to major chemical components, trace elements exhibit substantial variations, with their distribution regularly following the sampling profile from the distal to the most proximal zones of the Argemela intrusion (Supp. Table 2, detection limits and where to find standard analysis in Supp. Table 3). The proximal halo is characterised by an extreme increase in F, Li, and B contents (Fig. 10, top of the figure), along with a smaller rise in Be, As, Cs, and Bi (Fig. 10, mid-page plot) concentrations and, to a lesser extent, Sn and W (Fig. 10, bottom plot). Samples taken between 40 and 400 m in the semi-distal halo also show an increase in the concentration levels of these elements, but to a lesser extent (Fig. 10). On the other hand, the different chemical trace elements show virtually no significant variation. If we compare the spatial range at which anomalous concentrations are found for Sn and W, the distances around Argemela are between a few dozen and a few hundred meters.

In the proximal halo (0-20 m), boron and arsenic display the strongest enrichments, with concentration increases of up to 70-100× and 150-200× relative to background values, respectively. Lithium is enriched by a factor of approximately 40-70, whereas caesium, tin and tungsten show more moderate enrichments in the range of 15-30× . Beryllium and bismuth exhibit lower but still significant enrichment factors, of about 12-15× and ~ 5×, respectively. In the semi-distal halo (20-300 m), enrichment patterns are broadly similar but generally less pronounced. Boron, arsenic and lithium remain strongly enriched, whereas caesium, tin, tungsten, beryllium and bismuth show decreasing enrichment factors with

increasing distance from the intrusion. In the distal zone (300-3000 m), element concentrations are broadly comparable to regional background levels, with enrichment factors typically ranging between 0.5 and 2.

Compared with the nearby environment at Panasqueira, where the halo can be seen several kilometres away, the distances are smaller here, as there is no extended (and connected) fracture network with a large amplitude like that at Panasqueira. Fig. 11 shows the enrichment in F and Li of the proximal slates. Compared to the regional Beiras slates, the enrichment reaches a factor higher than 40 for Li, and above 20 for fluorine. Indicative thresholds of approximately 350 ppm Li and 2000 ppm F may be used to delimitate the abnormal values of the hydrothermal halo as indicated by the dashed lines from Fig. 11.

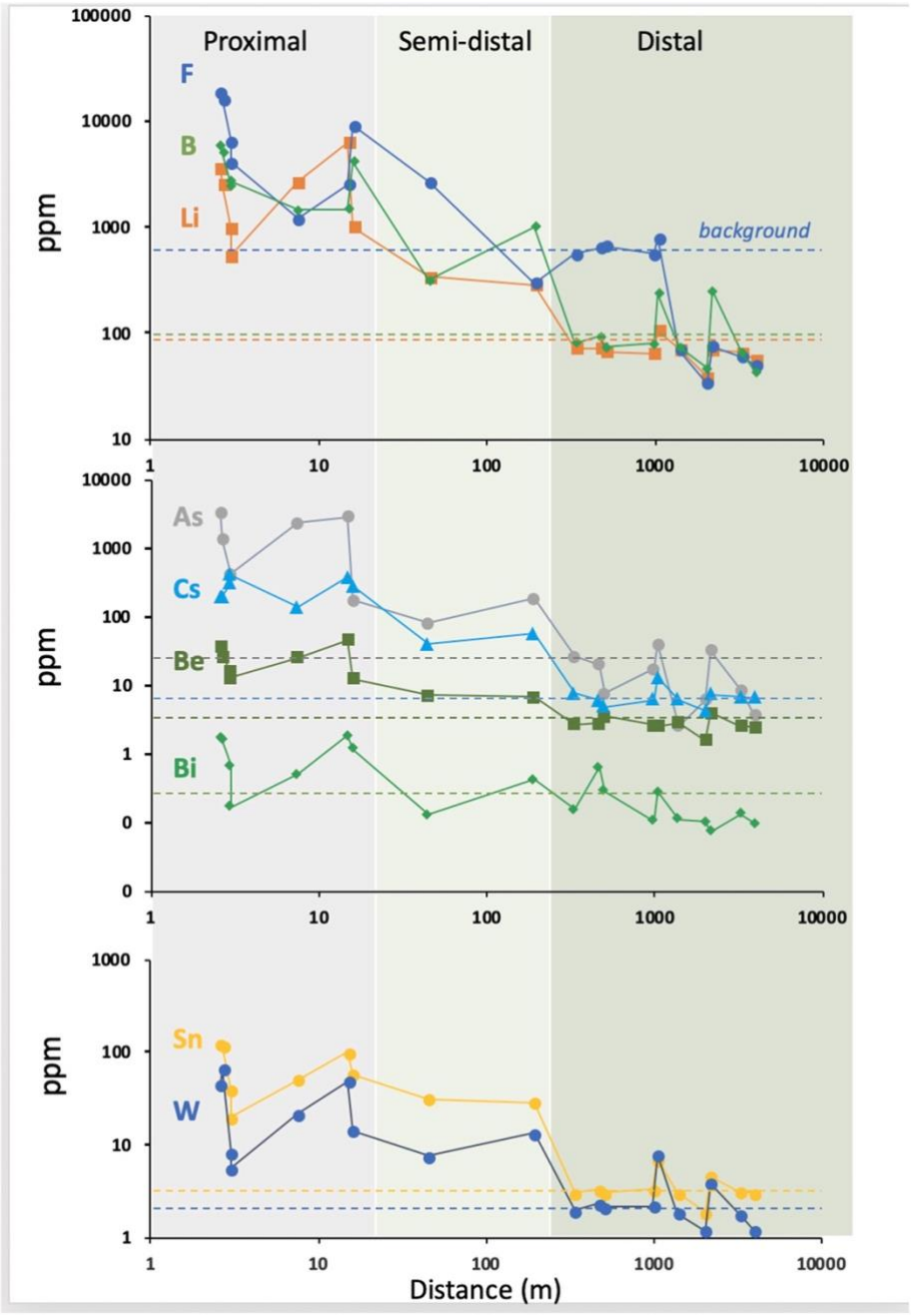

Fig. 10. Concentrations in F, B, and Li (a), and As, Be, Bi, and Cs (b) in slates (bulk rock analyses) as a function of distance to the Argemela intrusion. The analytical uncertainty for whole rock analyses is less than the data point size.

4.4. Main mineral crystal chemistry-trace elements in key minerals

The leading potential carriers of F (electron microprobe), Li, Rb, and Cs (by LA-ICP-MS) were studied. Micas were found to be the leading carriers of most of these elements. A significant change in concentrations along the sampling profile was detected, very similar to that recorded by whole-rock data. Fluorine in the micas analysed by EPMA reaches 3-4 wt% near the Argemela intrusion and 1-2.5 wt% between 200 and 40 m
from the intrusion. In contrast, it is close to the detection limits in distal samples (Supp. Table 4). In addition, micas from samples close to the intrusion (less than 20 m) are richer in iron and magnesium, less aluminous and richer in Si (Supp. Table 4), indicating a significant phengitic substitution.

About trace element concentrations measured by LA-ICP-MS (Fig. 12), muscovite, biotite, and chlorite, clearly identified petrographically in thin sections without ambiguity and of sufficient large size were selected in priority. Mixed analyses only occur where phyllosilicate grain size is smaller than the minimum LA-ICP-MS spot diameter (~30 μm), particularly in fine-grained slates. This concerns only some data points from Fig. 12 so-called matrix, where it is impossible to perform LA-ICP-MS at the scale of the very fine phyllosilicates.

Near the intrusion, Li concentrations in micas are higher than 1000 ppm (average around 2000-3000 ppm); Rb concentrations are also higher than 1000 ppm (average of 15,550 and 3000 ppm) compared with 30 to 180 ppm in the distal host slates, and Cs concentrations range from 100 to 400 ppm compared with the 1 to 10 ppm interval displayed by micas in slate samples far away of the Argemela intrusion. Sn has concentrations of 70 to 300 ppm, compared with a few ppm in the far- distant slates, and W shows concentrations of 20 to 30 ppm, very close to the intrusion, compared with a few ppm beyond (Supp. Table 5).

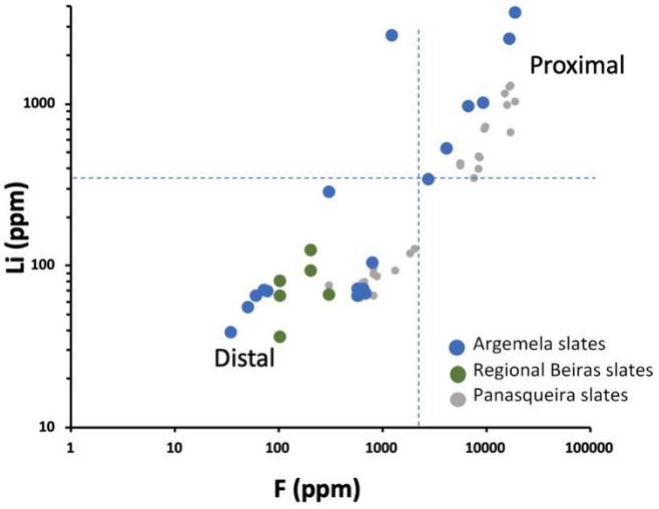

Fig. 11. Binary plot Li vs F for slates hosting the Argemela intrusion and slates from the Panasqueira deposit and from regional slate outcrops not located near intrusions (unpublished data from MOSTMEG final report, Mateus et al., 2024).

5. Discussion

In many Iberian Variscan settings, it is hard to pinpoint the direct geochemical impact of granitic intrusions on nearby metasedimentary rocks because these intrusions were emplaced over long periods (around 315-295 Ma), mineralizing systems often form around the granite bodies and are structurally controlled, and mineralization-hydrothermal processes are typically multi-stage (often W at 310-315 Ma and Sn–W at 300 Ma or later). All these factors result in variable overprints of the original magmatic signals. That is why the Argemela case is remarkable, as it preserves a clear, lightly overprinted alteration halo, allowing a direct look at the interaction between granite-derived fluids and host rocks during the intrusive plug emplacement. In addition, considering that the study sector is characterised by a very low density of mineralized structures, the S_0-S_1 fabric represents the main local control of rock permeability, providing a pervasive structural network that controls fluid-rock interaction and explains the lateral continuity of the observed alteration halo.

5.1. Mineralogical and geochemical zonation around the intrusion

From the point of view of the layout of the modified slates, the geometry around the Argemela intrusion can be summarised in three sections. The first section, adjoining the igneous body, corresponds to a proximal zone where the mineral paragenesis of the spotted slates is profoundly transformed via significant metasomatism. The latter process is characterised by an extreme increase in boron in the form of pervasive tourmalinization, as well as the recrystallisation of micas, particularly those enriched in F, Li, Cs, and Rb, which explains the high overall whole-rock contents in Li, B, F, Rb, and Cs. More moderate geochemical fingerprints are observed for Sn and W, as well as As, which are likely to be cryptic inclusions or trace constituents incorporated into the mica lattice. The second section is essentially a geochemical imprint, similar to the proximal zone in terms of the chemical elements involved. Even so, the concentration levels of these proxy elements are approxi- mately an order of magnitude lower than those recorded for the first section and are also about an order of magnitude higher than the average contents documented for the country slates. The third section corresponds to mottled slates without any sign of intrusion-related imprint and exhibits compositional features like those of the Beiras Group slates analysed elsewhere. Regarding the distribution of B, F, Li and Cs among host minerals, boron is almost entirely hosted by tourmaline, whereas Li, Cs and F are mainly incorporated into muscovite. Locally, biotite may also host Li and F, but its overall contribution re- mains limited compared to muscovite.

Muscovite is widely recognized a as a geochemical indicator of fluid composition and rare metal enrichment in granitic systems (e.g., Michaud and Pichavant, 2020; Dai et al., 2025; Kahou et al., 2026). It records both magmatic-hydrothermal processes within granites and fluid-rock interactions with surrounding host rocks, including the incorporation or redistribution of elements such as W, Li, Cs, and F (e.g., Xu et al., 2023). In the Argemela halo, muscovite primarily reflects recrystallization processes associated with fluid circulation, leading to the incorporation of Li, Cs and F released from the granite into newly formed micas within the host slates.

5.2. Significance of the metasomatism

The zonation observed around the intrusion is of a size compatible with the Argemela intrusion, a small, semi-vertical, sub-cylindrical body approximately 400 m in diameter with a known vertical extension of at least 500 m, as determined by geophysical studies (Michaud et al., 2020). Given its size and the volume involved, such an intrusion cannot develop very

significant chemical zonation. However, the intensity of the alteration recorded by slates in the vicinity of the igneous body indicates a vigorous expulsion of (chemically contrasting/reactive) fluids that intensely modify the host rocks over a few tens of meters and pervasively over a few hundred meters (distal aureole).

5.3. Significance of slate assemblages

The mineral parageneses linked to contact metamorphism are most probably related to an event that preceded the emplacement of the Argemela intrusion. It is still difficult to imagine such an extensive halo linked to the Fund˜ao pluton (late Cambrian-Early Ordovician in age), considering the observed field relationships. Therefore, the slate spots are conceivably tracing a concealed intrusion, as are the spotted slates outcropping at Panasqueira (15 km further west). This observation confirms the hypothesis formulated by Inverno et al. (2019). In the distal section, the spots are deformed, crenulated in samples ST2 and ST3, or ellipsoidal, as they are often described in other areas on a regional scale (Ribeiro da Costa et al., 2018). They underwent deformation, but they postdate the local D1 deformation and tectonic layering (S0//S1) in all situations. Such deformation is visible in the semi-distal zone, where spots display relics of euhedral shapes that are undeformed.

Potential temperature estimates can be inferred from the transition between mineral assemblages, as shown in Fig. 13. Existing thermody- namic models provide limited constraints at low-pressure conditions near the biotite-chlorite stability boundary. Mineral paragenesis therefore were therefore considered as remaining the most reliable simplistic approach here. The predominance of cordierite helps deter- mine the P-T conditions of the metamorphic aureole related to the inferred pluton at depth. Cordierite is considered a typical index mineral through the KFMASH divariant reaction (Pattison et al., 2002; Pattison and Vogl, 2005):

$$\text{Chlorite} + \text{Muscovite} + \text{Quartz} \rightarrow \text{Cordierite} + \text{Biotite} + H_2O$$

The temperature of the granite solidus is likely lowered by the sig- nificant quantities of B, F, and Li in the melt, as already demonstrated by the displacement to the left-hand side of the solidus curve down to temperatures in the range of 600-620 °C (Pichavant, 1981). Therefore, the temperature in the vicinity of the intrusion may have reached 550-600 °C near the contact. The cordierite then destabilised during the cooling path to muscovite + biotite and finally muscovite + chlorite at very low-pressure conditions. These conditions are inferred

from the most probable age range of the intrusion. The hypabyssal textures, the LCT character of the granite geochemical features, and the similarity with other RMG granites (Panasqueira: Marignac et al., 2020; Marignac and Cathelineau, 2023) are in favour of an intrusion linked to the late stage of the Variscan orogen (300-310 Ma) and synchronous with the exhumation of the CIZ belt.

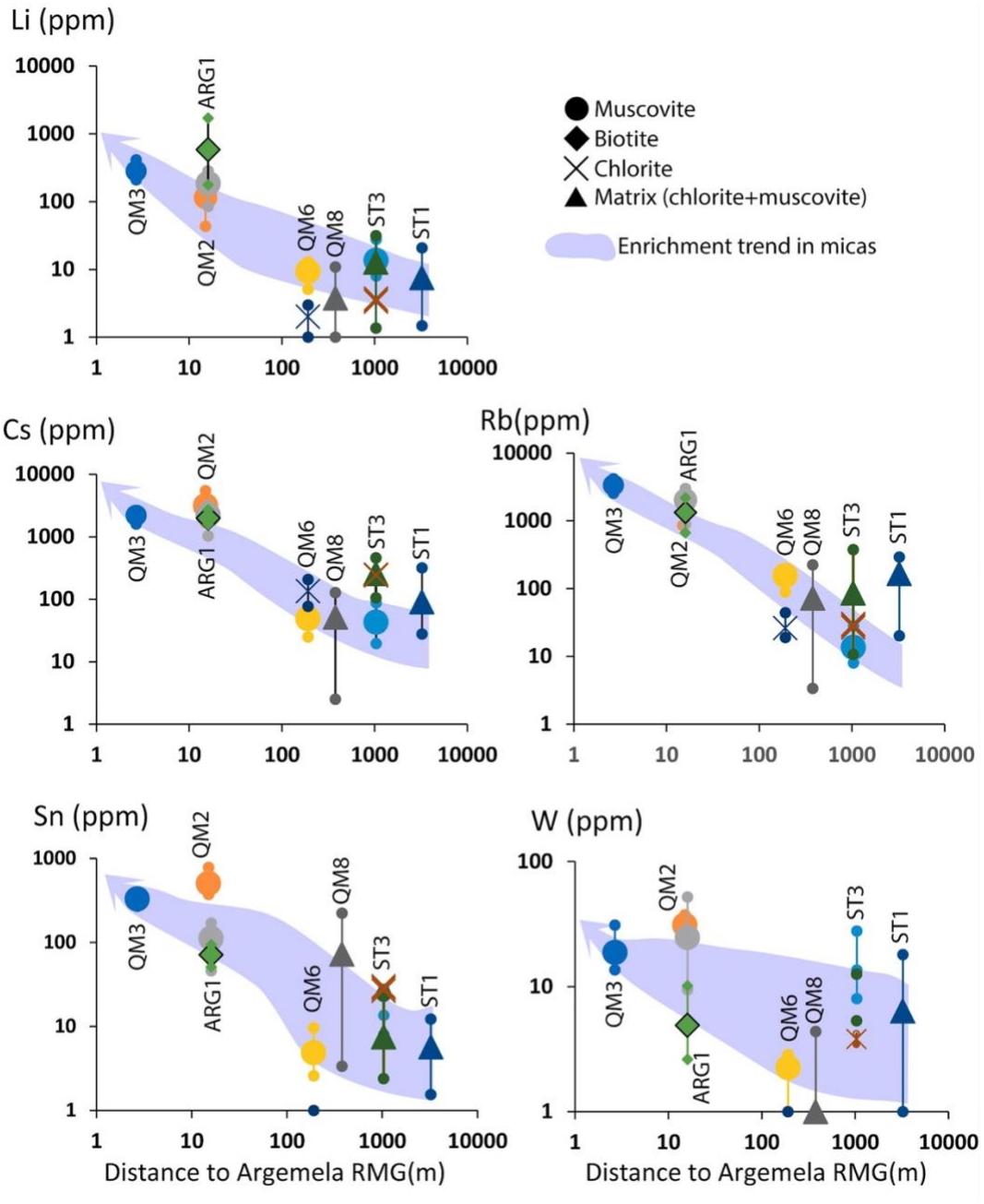

Fig. 12. Evolution of Li, Cs, Rb, Sn, and W concentrations in phyllosilicates, determined by LA-ICP-MS, as a function of distance to the Argemela intrusion. Trend as a light blue arrow. (For interpretation of the references to colour in this figure legend, the reader is referred to the web version of this article.)

5.4. Geochemical halos

The diagram in Fig. 14 shows that the slates in both the proximal and intermediate zones are enriched in Li and Rb, at concentration levels equivalent to those in the Argemela granites (Michaud and Pichavant, 2020). Therefore, it can be concluded that slates incorporate abundant fluorine and lithium and host the same mass of these elements as hyper-

differentiated granites themselves. The intrusion of the hyper- differentiated granite released a significant fluid volume that migrated through the shales thanks to matrix and fractured-controlled permeability (Fig. 14). The openness of the foliation planes, combined with a network of micro-fissures enabling the relay between planes, is at the origin of the highly branched tourmalinization textures in the proximal zones (Fig. 15). As mentioned by Inverno et al. (2019), fluid escaped from the Argemela intrusion or even from a subjacent intrusion that is not visible. These fluids disseminated significant tonnages of Li, Rb, and Cs, which were incorporated into the recrystallized micas at this stage.

Fig. 14 and Supp. Table 6 compare the hydrothermal haloes to the size of the spotted schist area, and the surface of the outcropping granites in four cases: the Regoufe, the Panasqueira, the Argemela and the Penamacor-Monsanto granites. In the case of Panasqueira, the intrusion is not outcropping but the greisenized-granite cupola is observed in underground mining works. In this specific case the volume of the intrusion, and the surface affected both by spotting, and hydro- thermal haloes is by far larger than in the other cases. The Penamacor- Monsanto develops very short contact metamorphic aureoles and almost no hydrothermal haloes. At the scale considered in Fig. 15 for Argemela, based on geochemical haloes, the dominant hydrothermal pathway in the immediate vicinity of the intrusion is the regional schistosity (S_1), developed during the main D1 deformation phase and transposing the original bedding (S_0). Later deformation phases (D2-D3) and associated brittle structures are poorly expressed in the studied sector and do not significantly control alteration zoning.

The temperature contrast between the intrusion and its fluids and the temperature of the host rock probably enabled the precipitation of quartz and tourmaline. Fluid-rock interaction experiments conducted by Orlando et al. (2017) show that a biotite schist in presence of B-bearing aqueous fluids at 500-600 °C and 100-130 MPa could convert in a tourmalinized rock when H_3BO_3 concentration in the fluid is greater than 1.6 M. Such a reaction is likely to have occurred in the first meters at the contact of the Argemela intrusion. These processes were already registered around several plutons or pegmatites in Portugal and Spain, the Fregeneda pegmatite being one of the best examples, where enclosing schists underwent metasomatism, resulting in a significant increase in Li (up to 4000 ppm gain), Cs and Rb (both up to 1300 ppm gain), and Sn (F, B) (Errandonea-Martin et al., 2022). In this example, the distance of enrichment is estimated to reach 4 to 5 times the thick- ness of the dykes. Such distances are not reached at Argemela, probably because the amount of fluids exsolved from the Argemela granite is less than the fluid volume exsolved from a pegmatite.

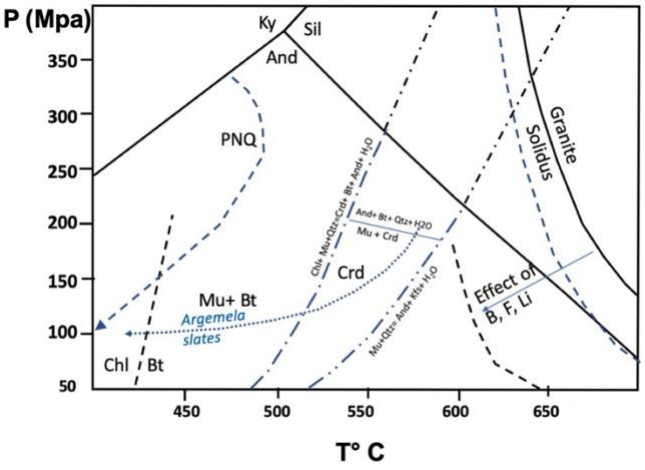

Fig. 13. P-T diagram showing stability fields of aluminium silicate polymorphs and main potential reactions between cordierite, biotite, muscovite, and chlo- rite. Granite solidus curves are from Festa et al. (2013) for a granodiorite, and from Pichavant (1981) for B-rich granite (blue dashed line). The arrow indicates the lowering of the temperature of the solidus because of fluxing elements (B, F, Li). PNQ: Panasqueira P-T evolution deduced from fluid inclusions data (Cathelineau et al., 2020). The dotted line labelled "Argemela" indicates the possible P-T evolution in the surroundings of the Argemela intrusion. (For interpretation of the references to colour in this figure legend, the reader is referred to the web version of this article.)

5.5. Reliable geochemical indicators and limitations in their use

From the study of Argemela intrusion hydrothermal halo, and similar haloes in Regoufe and Panasqueira from literature, it turns out that Li and F are reliable distal indicators. Of course, this consideration applies primarily in the case of peraluminous granitic systems intruding low- grade metasedimentary rocks, where background concentrations are low and mineralogical buffering is limited. Their applicability may be reduced in mafic protoliths, carbonate-rich sequences, or tectonically complex settings where fluid pathways dominate over diffuse metasomatism. Indicative thresholds of approximately 350 ppm Li and 2000 ppm F (Fig. 9) corresponding to the lowest values in the semi-distal zone can be proposed and discussed as first-order exploration criteria, while acknowledging that local background values must always be considered.

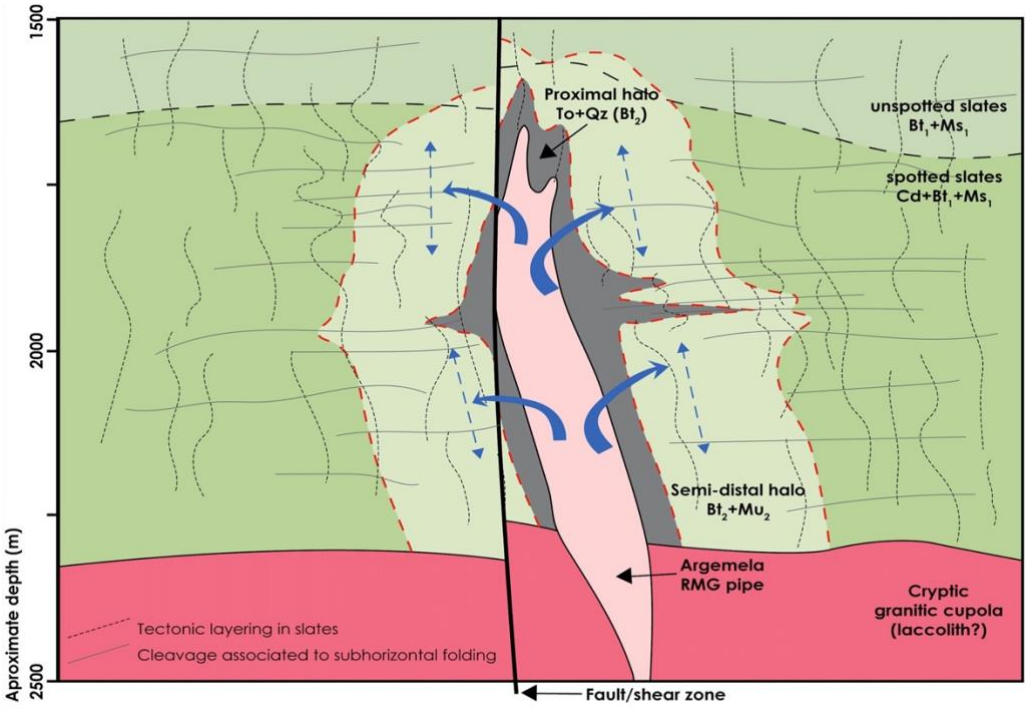

Fig. 14. Schematic cross-section of the Argemela rare metal granite (RMG) intrusion and the haloes of mineralogical and geochemical changes linked to the metasomatic effects of the fluids expelled from the intrusion.

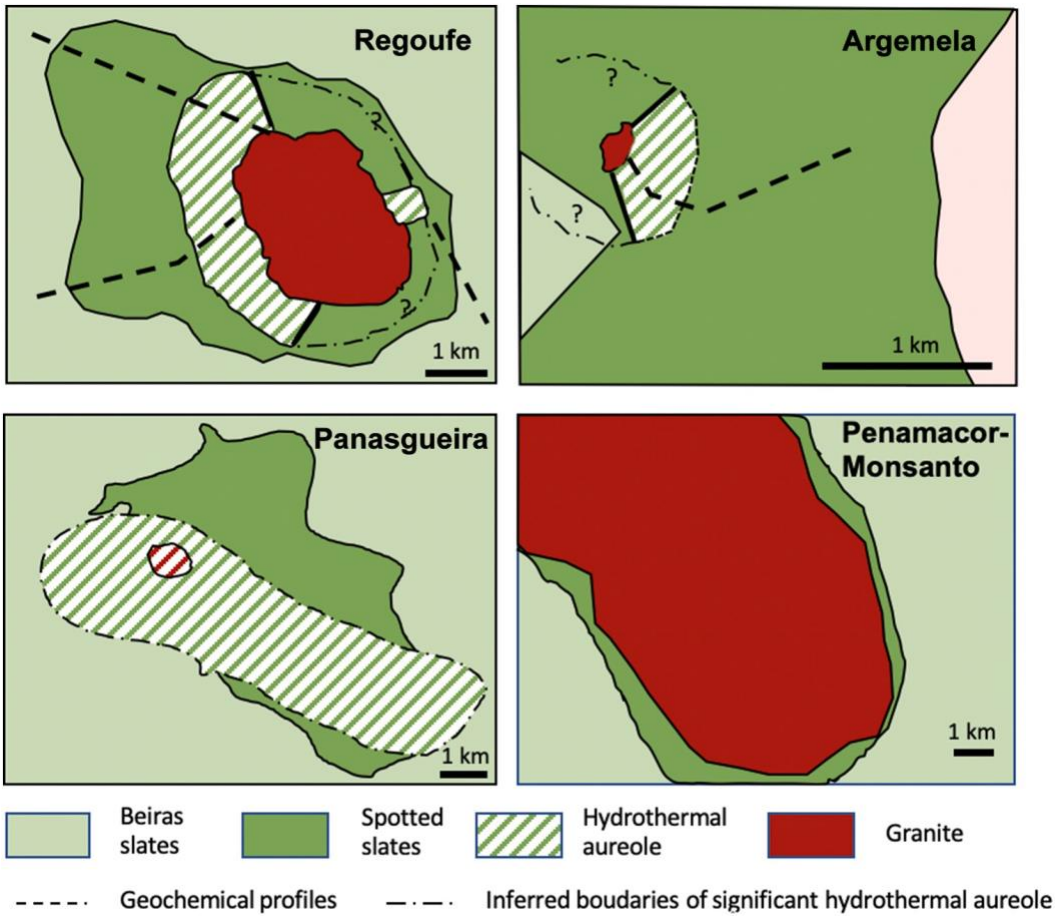

Fig. 15. Comparison of hydrothermal haloes, area of spotted slates, and size of the outcropping granites in the four case studies: Regoufe (data from Haar et al., 1993), Panasqueira (Gonçalves et al., 2018), Argemela (this work), and Penamacor (Ribeiro da Costa et al., 2018). In the case of Panasqueira, the greisenized-granite cupola intersected by underground mining works is represented in hatched red. (For interpretation of the references to colour in this figure legend, the reader is referred to the web version of this article.)

5.6. Perspectives for future mapping works

The novelty of the present study does not lie in individual methods, but in their combined application to a continuous profile from a small rare-metal granite into barren slates, allowing the spatial extent of diffuse metasomatism to be quantified. It can be emphasized

that almost no detailed description of spotted Beiras Group slate is available in literature, as well as the nature of the minerals replacing inferred cordierite. These spotted schists were deeply affected by a zoning including complete replacement by quartz and tourmaline at the very contact of the intrusion, a distal halo with recrystallized matrix and spots into a muscovite-biotite assemblage now retrogressed to muscovite+ chlorite.

Lateral extension of the hydrothermal aureole as shown in Fig. 15 is limited by the existing data base on a single profile. Vertical geochemical profiles from drill cores are indeed absent, as no boreholes are available at sufficient distance from the intrusion, and no vertical sampling of the enclosing rocks exists. The vertical extent of the halo remains unconstrained. However, based on gravimetric data indicating a subvertical pipe-like intrusion with a subrounded section, the alteration halo is likely to form a cylinder of approximately constant diameter at depth. To better understand the geometry of the aureole, field- based and airborne spectroscopic mapping techniques, using either portable instruments or airborne platforms (drones, aircraft), offer promising solutions to overcome the intrinsic limitations of sampling profiles, which are constrained by sample density and analytical costs. In the context of Li-F-Cs anomalies related to intense muscovitization of metasedimentary rocks surrounding rare-metal granitic intrusions, several perspectives can be envisaged for future exploration-oriented studies.

Recent developments have demonstrated that lithium, a light element not detectable by conventional X-ray fluorescence methods (limited to elements heavier than Na), can be mapped using Laser- Induced Breakdown Spectroscopy (LIBS). Studies by Fabre et al. (2021, 2022), Capela et al. (2025) and Harmon et al. (2025) have shown that LIBS provides reliable Li detection at the outcrop scale, making this technique particularly suitable for mapping Li anomalies in Beiras-type schist formations affected by granite-related metasomatism.

An alternative and complementary approach consists in mapping the alteration assemblages defined in this study, notably the intensity of muscovitization and, locally, tourmalinization in proximity to the intrusion. Several studies have demonstrated the efficiency of infrared reflectance spectroscopy for delineating hydrothermal alteration halos. Sun et al. (2001), using a Portable Infrared Mineral Analyser (PIMA), successfully discriminated white mica, chlorite and carbonate assemblages associated with hydrothermal alteration zones adjacent to base- metal sulfide deposits at the Elura Mine (Australia), based on variations in absorption

band position and intensity. Similarly, Yang et al. (2011) showed that short-wave infrared spectra acquired with a PIMA-II in- strument could resolve spatial variations in white mica composition (from phengite to muscovite) within hydrothermal alteration halos at the Hellyer massive sulphide deposit. More recently, hyperspectral visible-near infrared (VNIR), short-wave infrared (SWIR) and thermal infrared (TIR) data have been combined with multivariate and machine- learning approaches to extract quantitative geochemical information.

Laukamp et al. (2023) demonstrated that Partial Least Squares-based modelling of hyperspectral drill-core data allows the estimation of key geochemical indices (e.g., Mg#, ASI), enabling stratigraphic correla- tions and alteration mapping at depth. In a similar perspective, Murer and de Souza Filho (2026) showed that VNIR-SWIR spectral databases coupled with machine-learning models can predict rare earth element contents with significant confidence.

Together, these studies indicate that reflectance spectroscopy, especially when integrated with targeted geochemical analyses and data-driven modelling, represents a powerful tool for quantifying the spatial extent of geochemical and mineralogical aureoles around con-cealed or weakly exposed granitic intrusions. Such approaches would represent a natural extension of the results presented here.

6. Conclusions

The intrusion of the hyper-differentiated Argemela granite has generated hyper-localised heat flow and released fluids, creating a hydrothermal system. The large volume of hydrothermal fluids released from the intrusion resulted in significant transformations of the Beiras Group slates.

Metasomatized quartz-tourmaline slates formed at the contact and a muscovite-biotite zone beyond at a semi-distance. The principal mineral assemblage currently observed in the latter section of the sampling profile is a muscovite-biotite assemblage (later chloritized) with ghosts (pinite) of pre-existing cordierite crystals, which cannot be considered as resulting from the contact metamorphic halo related to the exposed granites. Epigeny of the ghost is sequential and begins with biotite formation at the external rim, with progressive invasion of the core, followed by extended muscovite replacement of the core.

A spectacular, abrupt geochemical and mineralogical zonation of transformations over relatively short distances is recorded from granite contacts in the host rocks: a silicified zone with tourmaline and muscovite development, a muscovite zone with minor tourmaline, and beyond, the spot slates show the usual mineralogy. The slates in this distal area are characterised by successive complex transformations involving superimposed metamorphic and hydrothermal histories: i) a cordierite spotting related to a hidden granite at shallow depths, at less than 1 km, ii) development of newformed biotite and muscovite linked to Argemela hydrothermal fluids, and complete retro-metamorphosis of the cordierite spots into a mica+ biotite assemblage, iii) path to the chlorite field due to the temperature decrease. The main mineral assemblage currently observable, apart from a few rare, scattered relics (biotite, cordierite), is a muscovite-chlorite assemblage. It should be noted that there is no clear metamorphic contact aureole, as for kilometres, the slates show spots that are not linked to the outcropping in- trusions (Argemela, Fund˜ao to the east-southeast, or Serra de Estrela granites to the north), which may indicate the presence of other intrusive plutonic bodies at depth, more extensive than the exposed granites.

Within a few hundred meters of the contact, the slates exhibit increased concentrations of Li, F, Sn, Cs, and Rb resulting from mica recrystallisation, and an increased B concentration due to pervasive tourmalinization. Fluorine and lithium concentrations appear to be good indicators of the proximity of granite intrusions at distances that exceed the significant

metasomatic impact observed in the first 10 m, where substantial transformations in the host series of Beiras slates occurred. Near the Argemela intrusion, concentrations of B, Li, F, Sn, Cs, and Rb (W) are exceptionally high in the metasomatized spotted slates. The effects identified at close distance diminish sharply with distance from the contact. However, there is still a plateau of several hundred meters before concentrations return to the level of the non-modified regional slates that form the Malpica do Tejo Formation (Beiras Group).

Fluorine and lithium concentrations in muscovite, which are very high close to the intrusion, are reasonably good indicators of the proximity of fertile RMG intrusions at distances that exceed the significant metasomatic impact observed within 10 m of the contact with the intrusion.

Funding

ERAMIN2 funded this research through the project MOSTMEG (htt p://doi.org/10.54499/ERA-MIN/0002/2019; https://mostmeg.rd. ciencias.ulisboa.pt/). This work contributes to a better knowledge of granite-related ore systems, namely those enriched in lithium. The research carried out within the framework of the Labex Ressources21 programs, under the reference ANR-10-LABX-21-RESSOURCES21, is supported by the Agence Nationale de la Recherche through the national "Investissements d'avenir" program, which contributes to the co-funding of the ERAMIN project. Analyses were carried out at the SCMEM and LA- ICP-MS platforms of GeoRessources in Nancy, which are funded by the Labex Ressources 21 (ANR-10-LABX-21-RESSOURCES21), the Région Lorraine, and the European Community through the FEDER program. The Portuguese Fundaçã˜o para a Ci ˆencia e a Tecnologia (FCT) provided additional support. I.P./MCTES through the PIDDAC national funds UIDB/50019/2020, LA/P/0068/2020; (https://doi.org/10.544 99/UIDB/50019/2020; https://doi.org/10.54499/LA/P/0068/2020) and PD/BD/142783/2018. IDS acknowledges the financial support of the researcher contract in FCUL funded by FCT 'Estímulo ao Emprego Científico- Norma Transitória' DL57/2016/CP1479/CT0030 (https:// doi.org/10.54499/DL57/2016/CP1479/CT0030a).

Declaration of competing interest

The authors declare that they have no known competing financial interests or personal relationships that could have appeared to influence the work reported in this paper.

Acknowledgments

A. Lecomte and O. Rouer (GeoRessources) are warmly acknowledged for their help when acquiring the SEM and EMPA. Two anonymous re- viewers are thanked for their valuable comments, and the editor for handling the manuscript and improvement suggestions.

Appendix A. Supplementary data

Supplementary data to this article can be found online at https://doi.org/10.1016/j.gexplo.2026.108068.

References

Antunes, I.M.H.R., Neiva, A.M.R., Corfu, F., 2012. U-Pb early Ordovician emplacement ages and K-Ar Variscan recrystallization ages of the Funda˜o granitic pluton, Central Portugal. In: European Mineralogical Conference, 1. EMC2012-747.

Arrykul, S., Drake, N., Dunlop, A.C., Govett, G.J.S., 1988. A comparison of drainage sediment and rock-geochemical surveys for sheeted-vein tin mineralisations near

Emmaville, N.S.W. Australia. J. Geochem. Expl. 30, 123–144.

Breiter, K., Dˇ uriˇsov´a, J., Korbelov´a, Z., Lima, A., Vaˇsinov´a Galiova´, M., Hloˇzkova´, M., Dosbaba, M., 2022. Rock textures and mineral zoning – a clue to understanding rare-metal granite evolution: Argemela stock, Central-Eastern Portugal. Lithos 410–411,106562. https://doi.org/10.1016/j.lithos.2021.106562.

Bussink, R.W., 1984. Geochemistry of the Panasqueira tungsten-tin deposit, Portugal.Geol. Ultraiect. 33, 170.

Capela, D., Lopes, T., Dias, F., Ferreira, M.F.S., Teixeira, J., Lima, A., Jorge, P.A.S., Silva, N.A., Guimar˜aes, D., 2025. Advancing automated mineral identification through LIBS imaging for lithium-bearing mineral species. Spectrochim. Acta B At. Spectrosc. 223, 107085. ISSN 0584-8547. https://doi.org/10.1016/j.sab.2024.107085.

Carignan, J., Hild, P., Mevelle, G., Morel, J., Yeghicheyan, D., 2001. Routine analyses of trace elements in geological samples using flow injection and low-pressure on-line liquid chromatography coupled to ICP-MS: a study of geochemical referencematerials BR, DR-N, UB-N, AN-G and GH. Geostand. Newslett. 25, 187–198. https://doi.org/10.1111/j.1751-908X.2001.tb00595.x.

Cathelineau, M., Boiron, M.C., Marignac, C., Dour, M., Dejean, M., Carocci, E.,

Truche, L., Pinto, F., 2020. High pressure and temperatures during the early stages of tungsten deposition at Panasqueira revealed by fluid inclusions in topaz. Ore Geol. Rev. 126, 103741.

Cathelineau, M., Boiron, M.-C., Lecomte, A., Martins, I., Dias Da Silva, ´I., Mateus, A.,2024. Lithium-, phosphorus-, and fluorine-rich intrusions and the phosphate sequence at Segura (Portugal): a comparison with other hyper-differentiated magmas. Minerals 14, 287. https://doi.org/10.3390/min14030287.

Charoy, B., Noronha, F., 1996. Multistage growth of a Rare-Element, Volatile-RichMicrogranite at Argemela (Portugal). J. Petrol. 37, 73–94.

Chork, C.Y., 1990. Unmasking multivariate anomalous observations in exploration geochemical data from sheeted-vein tin mineralisation near Emmaville, N.S.W.,Australia. J. Geochem.

Explor. 37, 205–224.

Codeço, M.S., Weis, P., Trumbull, R.B., Van Hinsberg, V., Lecumberri-Sanchez, P., Schleicher, A.M., 2021. The imprint of hydrothermal fluids on trace-elementcontents in white mica and tourmaline from the Panasqueira W–Sn–Cu deposit,Portugal. Mineral. Deposita 56, 481–508.

Dai, H.T., Zhang, Y., Pan, J.Y., Xia, F., Ma, T., Xu, Z., Han, S.C., Liu, G., Zhong, F.J., Zhang, X.T., Yan, J., Zhang, S.Y., Zhang, X., Du, G.F., 2025. Li mineralization processes in the Gaoaobei W-Li deposit, Nanling, South China: evidence from chemical compositions of mica and cassiterite U-Pb dating. Ore Geol. Rev. 183,106647.

Errandonea-Martin, J., Garate-Olave, I., Roda-Robles, E., Cardoso-Fernandes, J., Lima, A., Ribeiro, M.d.A., Teodoro, A.C., 2022. Metasomatic effect of Li-bearing aplite-pegmatites on psammitic and pelitic metasediments: geochemical constraintson critical raw material exploration at the Fregeneda–Almendra Pegmatite Field

(Spain and Portugal). Ore Geol. Rev. 150, 105155.

Fabre, C., Ourti, N.E., Mercadier, J., Cardoso-Fernandes, J., Dias, F., Perrotta, M., Koerting, F., Lima, A., Kaestner, F., Koellner, N., Linnen, R., Benn, D., Martins, T., Cauzid, J., 2021. 596, Analyses of Li-Rich Minerals Using Handheld LIBS Tool. Data6, 68.597. https://doi.org/10.3390/data6060068.

Fabre, C., Ourti, N.E., Ballouard, C., Mercadier, J., Cauzid, J., 2022. Handheld LIBS analysis for in situ quantification of Li and detection of the trace elements (Be, Rb and Cs). J. Geochem. Explor. 236, 106979. https://doi.org/10.1016/j. gexplo.2022.106979. hal-03673941.

Ferreira da Silva, A., 2013. A Litostratigrafia e Estrutura do Supergrupo Dúrico-Beira˜o(Complexo Xisto-Grauv´aquico), em Portugal, e sua correlaça˜o com ascorrespondentes sucesso˜es em Espanha. Bol. de Minas 48, 97–142.

Festa, V., Caggianelli, A., Langone, A., Prosser, G., 2013. Time-space relationships among structural and metamorphic aureoles related to granite emplacement: a case studyfrom the Serre Massif (southern Italy). Geol. Mag. 150, 441–454.

Gonçalves, M.A., Mateus, A., Pinto, F., Vieira, R., 2018. Using multifractal modelling, singularity mapping, and geochemical indexes for targeting buried mineralization: application to the W-Sn Panasqueira ore-system, Portugal. J. Geochem. Explor. 189,42–53.

Haar, A.J., Vriend, S.P., Van Gaans, P.F.M., 1993. Hydrothermal alteration of the Beira schists around the W-Sn specialised Regoufe granite, NW Portugal. J. Geochem.Explor. 46, 335–347.

Harmon, R.S., Lu, P.L., Curry, A.C., Murray, R.M., Richter, D.D., 2025. Libs as a tool for Li-pegmatite exploration and prospect evaluation: soil mica and soil analysis from the Carolina Tin-

Spodumene Belt. Appl. Geochem. 191, 106534. ISSN 0883-2927. https://doi.org/10.1016/j.apgeochem.2025.106534.

Inverno, C., Ribeiro, L., 1980. Fracturaça˜o e cortejo filoniano nas minas de Argemela. In:Comunicaço˜es Serviços Geolo´gicos de Portugal, 66, pp. 185–193.

Inverno, C., Ferraz, P., Moreira, M., Guimaraes, F., Filipe, A., 2019. The granite-related, high-tonnage Sn-Li deposit of Argemela, Central Portugal. In: Cadernos do Laboratorio Xeolo´xico de Laxe: Revista de xeoloxía galega e do Hercínico peninsular,41, pp. 201–256.

Kahou, Z.S., Cathelineau, M., Boiron, M.-C., Lecomte, A., Peiffert, C., Fullenwarth, P.,2026. From Fe Li rich micas to lepidolite and muscovite: the magmatic to hydrothermal evolution of phyllosilicates in the apical zone of the Beauvoir granite(French Massif Central). Lithos 524–525. https://doi.org/10.1016/j.lithos.2026.108418.

Kelly, W.C., Rye, R.O., 1979. Geologic, fluid inclusion, and stable isotope studies of thetin–tungsten deposits of Panasqueira, Portugal. Econ. Geol. 74, 1721–1822.

Large, R.R., McGoldrick, P.J., 1998. Lithogeochemical halos and geochemical vectors tostratiform sediment-hosted Zn–Pb–Ag deposits, 1. Lady Loretta Deposit, Queensland.J. Geochem. Explor. 63, 37–56.

Laukamp, C., Beattie, E., LeGras, M., 2023. Modelling geochemical indices from hyperspectral drill core data from the Eucla Basin basement. J. Geochem. Explor.253, 107293. https://doi.org/10.1016/j.gexplo.2023.107293.

Launay, G., Sizaret, S., Lach, P., Melleton, J., Gloaguen, E., Poujol, M., 2021. Genetic relationship between greisenization and Sn-W mineralizations in vein and greisen deposits: Insights from the Panasqueira deposit (Portugal). Bull. Soc. G´eol. Fr. 192, 2.

Lima, L., Guedes, A., Noronha, F., 2019. Tungsten mineralization associated with theArgemela microgranite (Central Portugal). J. Iber. Geol. 1–16. https://doi.org10.1007/s41513-019-00113-z.

Longerich, H.P., Jackson, S.E., Günther, D., 1996. Inter-laboratory note. Laser ablation inductively coupled plasma mass spectrometric transient signal data acquisition andanalyte concentration calculation. J. Anal. At. Spectrom. 11, 899–904.

Marignac, C., Cathelineau, M., 2023. The W Deposit at Panasqueira (Portugal): a critical Bibliographical Review. In: Metallic Resources 1: Geodynamic Framework and Remarkable Examples in Europe. Wiley, ISTE. https://doi.org/10.1002/9781394264810.

Marignac, C., Cuney, M., Cathelineau, M., Lecomte, A., Carocci, E., Pinto, F., 2020. The Panasqueira rare metal granite suites and their involvement in the genesis of theworld-class Panasqueira W–Sn–Cu vein deposit: a petrographic, mineralogical, andgeochemical

study. Minerals 10, 562.

Marques, F.O., Mateus, A., Tassinari, C., 2002. The Late-Variscan fault network inCentral–Northern Portugal (NW Iberia): a re-evaluation. Tectonophysics 359,255–270. https://doi.org/10.1016/S0040-1951(02)00514-0.

Martins, I., Mateus, A., Cathelineau, M., Boiron, M.C., Ribeiro da Costa, I., Dias daSilva, ´I., Gaspar, M., 2022. The Lanthanide "Tetrad effect" as an Exploration Tool forGranite-Related rare Metal Ore Systems: examples from the Iberian Variscan Belt. Minerals 12, 1067.

Mateus, A., Figueiras, J., Martins, I., Rodrigues, P.C., Pinto, F., 2020. Relative Abundance and Compositional Variation of Silicates, Oxides and Phosphates in the W-Sn-Rich Lodes of the Panasqueira Mine (Portugal): Implications for the Ore-Forming Process. Minerals 10, 551. https://doi.org/10.3390/min10060551.

Mateus, A., Cathelineau, M., Tassinari, C., Boiron, M.-C., Hollanda, M.H., Salgueiro, R., Guedes, A., Moita, P., Pereira, A., 2024. Final Report of the Eramin 2 European Contract MOSTMEG: Predictive Models for Strategic Metal-rich, Granite-related Ore Systems Based on Mineral and Geochemical Fingerprints and Footprints. https://m ostmeg.rd.ciencias.ulisboa.pt.

Meireles, C.A., 2020. Folha 4 da Carta Geolo´gica de Portugal, na escala 1:200 000. LNEG,Lisboa.

Michaud, J.A.-S., 2019. Rare Metal Granites: Origin, Emplacement and Mechanisms of the Magmatic Hydrothermal Transition. Insights From the Argemela Rare Metal Granite (Portugal) and an Experimental Study. PhD thesis. University of Orl´eans,365 p.

Michaud, J.A.-S., Pichavant, M., 2020. Magmatic fractionation and the magmatic- hydrothermal transition in rare metal granites; evidence from Argemela (CentralPortugal). Geochim. Cosmochim. Acta 289, 130–157. https://doi.org/10.1016/j.gca.2020.08.022.

Michaud, J.A.-S., Gumiaux, C., Pichavant, M., Gloaguen, E., Marcoux, E., 2020. From magmatic to hydrothermal Sn-Li-(Nb-Ta-W) in the Argemela area (Central Portugal). Ore Geol. Rev. 116, 103215.

Murer, Y.C., de Souza Filho, C.R., March 2026. VNIR-SWIR spectroscopy and machine learning: a new approach for rare Earth Element detection and quantification in fluorapatite veins (Nolans Bore Deposit, Australia). J. Geochem. Explor. 282,107955. https://doi.org/10.1016/j.gexplo.2025.107955.

Oosterom, M.G., Bussink, R.W., Vriend, S.P., 1984. Lithogeochemical studies of aureoles around the Panasqueira tin-tungsten deposit, Portugal. Mineral. Deposita 19,83–288.

Orlando, A., Ruggieri, G., Chiarantini, L., Montegrossi, G., Rimondi, V., 2017.Experimental Investigation of biotite-rich schist reacting with B-bearing fluids at upper crustal conditions and correlated tourmaline formation. Minerals 7, 155. https://doi.org/10.3390/min7090155.

Pattison, D.R.M., Vogl, J.J., 2005. Contrasting sequences of metapelitic mineral assemblages in the aureole of the tilted Nelson Batholith, British Columbia: implications for phase equilibria and pressure determination in Andalusite-Sillimanite-Type settings. Can. Mineral. 43, 51–88.

Pattison, D.R.M., Spear, F.S., Debuhr, C.L., Cheney, J.T., Guidotti, C.V., 2002.Thermodynamic modelling of the reaction muscovite + cordierite→Al2 SiO5 +biotite + quartz + H2O: constraints from natural assemblages and implications forthe metapelitic petrogenetic grid. J. Metamorph. Geol. 20, 99–118.

Patton, C., Hellstrom, J., Paul, B., Woodhead, J., Hergt, J., 2011. Iolite: Freeware for the visualisation and processing of mass spectrometric data. J. An. Atom. Spectr. 26,2508–2518.

Pichavant, M., 1981. An experimental study of the effect of Boron on a water-saturated haplogranite at 1 Kbar vapour pressure. Geological applications. Contrib. Mineral.Petrol. 76, 430–439.

Pinto, F.M., 2014. Estudo da distribuiça˜o do Estanho na Mina da Panasqueira.Dissertation,. Universidade do Porto. https://sigarra.up.pt/fmup/pt/pub_geral.pubview?pi_pub_base_id=34260.

Polya, D.A., 1989. Chemistry of the main-stage ore-forming fluids of the Panasqueira W- Cu (Ag)-Sn deposit, Portugal: implications for models of ore genesis. Econ. Geol. 84,1134–1152.

Polya, D.A., Foxford, K.A., Stuart, F., Boyce, A., Fallick, A.E., 2000. Evolution andparagenetic context of low δD hydrothermal fluids from the Panasqueira W-Sndeposit, Portugal: new evidence from microthermometric, stable isotope, noble gas and halogen analyses of primary fluid inclusions. Geochim. Cosmochim. Acta 64,3357–3371.

Portugal Ferreira, M., Costa, V., Regˆencio Macedo, C., Gama Pereira, L.C., 1977.Dataço˜es K-Ar em biotites das rochas granitoides da Cova da Beira (PortugalCentral). Mem. Not. Mus. Lab. Miner. Geol. Univ. Coimbra 84, 39–48.

Puchner, C.C., 1986. Geology, alteration, and mineralisation of the Kouga rock deposit,Seward Peninsula. Alaska. Econ. Geol. 81, 1775–1794.

Ribeiro da Costa, I., Antunes, I.M.H.R., Moura˜o, C., Recio, C., Guimaraes, F., Farinha Ramos, J., Barriga, F., 2018. Contact metamorphism associated to the Penamacor–Monsanto granitic intrusion (Central Portugal): geochemical, isotopic and mineralogical features. J. Iber. Geol. 44 (2018), 335–353. https://doi.org/ 10.1007/s41513-018-0050-x.

Ribeiro, R.F., 2017. Gravimetric Modelling and Geological Interpretation of Argemela–Panasqueira Area. MSc thesis,. University of Porto. Roma˜o, J., Ferreira da Silva, A., Proença Cunha, P., Pereira, A., Brito, A., 2010.

Esperancinha, A. Carta Geolo´gica de Portugal `a escala 1:50.000, Folha 25-CD

Rosmaninhal/Segura e 29-A Retorta, 1 edn. Laborato´rio Nacional de Energia e Geologia, Lisboa.

Santare´m, R., 1983. Interpretaç˜ao fotogeolo´gica da regi˜ao centro de Portugal. Estruturas circulares e fracturas com base em imagens do Sat´elite Landsat 2. In: Estudos, Notas e Trabalhos do Serviço de Fomento Mineiro, 25, pp. 227–245.

Sant'Ovaia, H., Olivier, P., Ferreira, N., Leblanc, D., 2010. Magmatic structures and kinematics of the emplacement of the Variscan granites from Central Portugal (Serra da Estrela and Castro Daire areas). J. Struct. Geol. 32, 1450–1465.

Sousa, M.B., 1983. Consideraço˜es paleogeogra´ficas e ensaio de correlaça˜o das formaço˜es do Grupo do Douro (CXG) com as formaço˜es ante-Ordovícias da Zona Centro-Ib´erica. Mem. Not. Mus. Lab. Miner. Geol. Univ. Coimbra 96, 65–98.

Sun, Y., Seccombe, P.K., Yang, K., September 2001. Application of short-wave infrared spectroscopy to define alteration zones associated with the Elura zinc–lead–silver deposit, NSW, Australia. J. Geochem. Explor. 73 (Issue 1), 11–26. https://doi.org/ 10.1016/S0375-6742(01)00167-4.

Uribe-Mogollon, C., Maher, K., 2018. White mica geochemistry of the copper cliff porphyry cu deposit: insights from a vectoring tool applied to exploration. Econ. Geol. 113, 1269–1295.

Xu, Z., Zhang, Y., Pan, J.Y., Zhang, F.S., Xia, F., Wu, Z.C., Han, S.C., Liu, G.Q., Zhong, F.J., Zhang, X.T., Liu, Y., Yan, J., Zhang, F.R., 2023. In situ LA-ICP-MS analyses of muscovite: constraints on granite-type Li mineralization in northwestern Jiangxi. South China. Ore Geol. Rev. 156, 105402.

Yakovenko, A., Guedes, A., Noronha, F., Dias da Silva, ´I., Mateus, A., 2025. P-T-X evolution of the fluids associated with Sn-li mineralization from Pedra Alta(Argemela, Portugal). J. Iber. Geol. https://doi.org/10.1007/s41513-025-00289-7.

Yang, K., Huntington, J.F.,Gemmell, J.B., Scott, K.M., 2011. Variations in composition and abundance of white mica in the hydrothermal alteration system at Hellyer, Tasmania, as revealed by infrared reflectance spectroscopy. J. Geochem. Explor. 108 (2), 143–156. https://doi.org/10.1016/j.gexplo.2011.01.001.